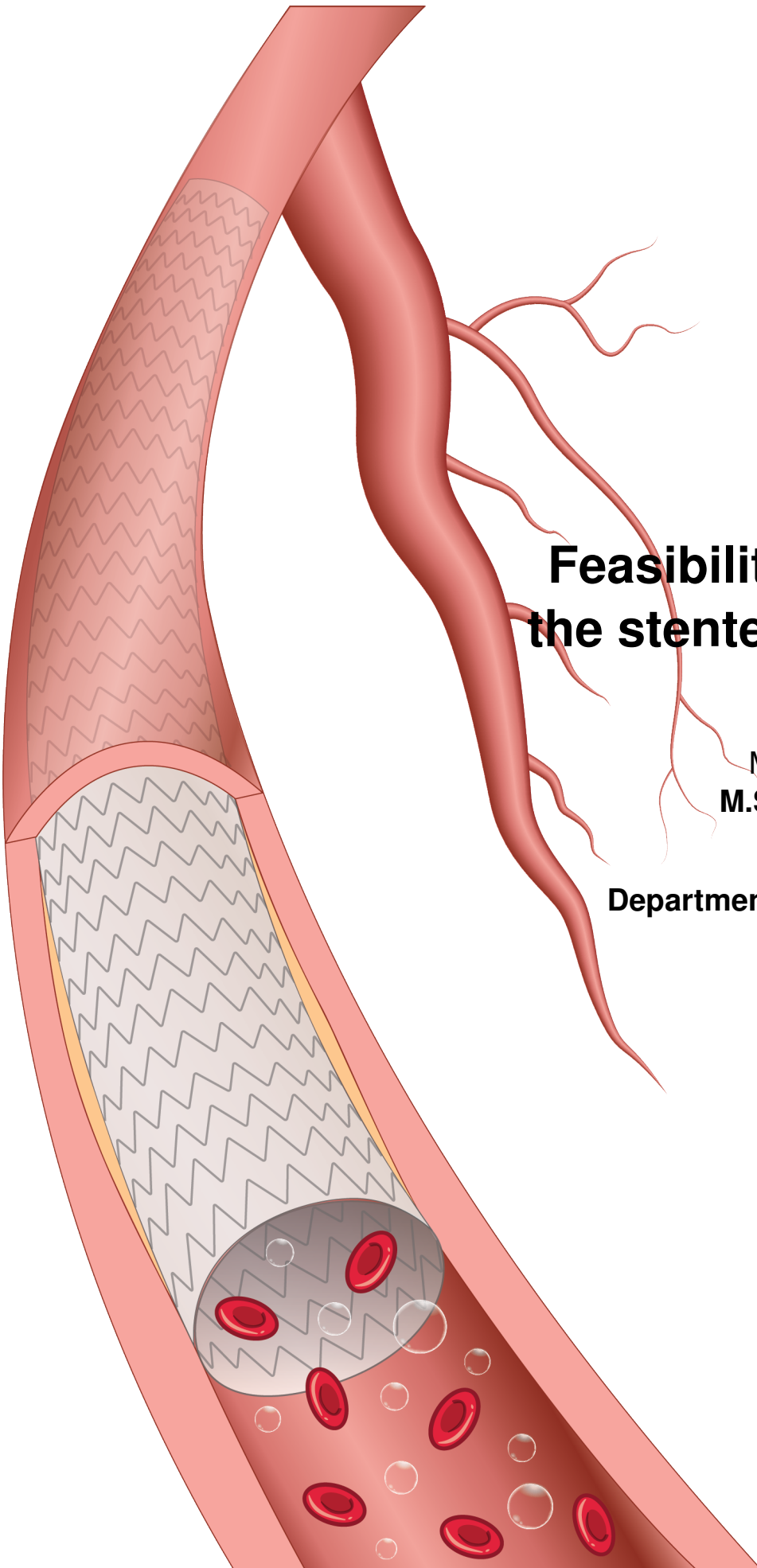


**Feasibility of echoPIV in
the stented femoral artery**

Master thesis
M.S. van der Vee

Department of Vascular Surgery
October 2018



Feasibility of echoPIV in the stented femoral artery

M.S. van der Vee

Colloquium

Date	Friday, October 5 th
Time	15:00
Location	University of Twente, Noordhorst 115

Graduation committee

Chair & Technical Supervisor	Prof. dr. M. Versluis
Medical Supervisor	Prof. dr. M.M.P.J. Reijnen
Daily Supervisor	Dr. E. Groot Jebbink
Mentor	Drs. R.J. Haarman
External Member	Dr. A.T.M. Bellos - Grob

Preface

This thesis is the result of my MSc graduation internship for the mastertrack Medical Sensing and Stimulation that belongs to the Master's programme Technical Medicine. I have enjoyed working at the department of vascular surgery of the Rijnstate Hospital located in Arnhem. My research goal was to set up and perform a clinical study focusing on the visualisation of bloodflow around stents. In this process, I found myself assisting in the operating room wondering if I should become a medical doctor, while the other day I was performing hydrophone measurements in the lab of the University of Twente. It was a remarkable year where I could learn and combine the best of both worlds. Still, I am glad that I could keep my research clinically focused which resulted in performing patient measurements.

I welcome this opportunity to thank friends, family and colleagues who provided help, guidance and support last year. First of all, I would like to thank all my supervisors. I am very grateful that I could always approach you with questions and that you encouraged me to reach my goals. I would like to thank Michel for the support and guidance, both academically and clinically. You are optimistic, curious and critical and your enthusiasm in vascular research was essential in keeping me motivated. With Michel, you formed an excellent team during the M&M meetings which I enjoyed. Michel, thank you for the technical guidance and asking the unexpected questions that brought my research to a higher level of success. Erik, thank you that you always made time to help and that I could always express my ideas. I learned a lot from you about performing good research. Rian, thank you for all the guidance during the last 2.5 years, I really enjoyed the 'intervisie' meetings. But most of all, I am forever grateful that I learned to reflect on myself, to be more open and express my feelings, even if they were complicated.

I would like to thank everybody who was involved in the echoPIV meetings at the Erasmus MC. You were bringing me new perspectives, and lots of valuable work to think about. In particular Jason, I am grateful that I could learn so much from you. Guillaume, thank you for your technical assistance and your patience to explain me. Your help throughout the year was very useful. Jorinde, thank you for the introduction with the Verasonics and helping me with the hydrophone measurements. My acknowledgements would not be complete without thanking Sophie and everybody from the Medical UltraSound Imaging Center of the Radboud UMC for your help with the PVA phantom.

Working with everybody in the Rijnstate hospital was fun. I would like to thank the other researchers for the productive but pleasant days. And off course, for all the lunch, coffee and cake moments. I would like to thank Cora, Jan-Willem, Luuk, and Steven, and all surgical residents for helping me in my clinical development. Furthermore, I would like to thank Daphne, Michelle and all the vascular sonographers for your help with the clinical study. Thank you Lennart, your flow perspective was always helpful. Stefan, you have been a continuing source of encouragement and optimism through-

out. I enjoyed our Verasonics sessions and your life lessons about Dragon Ball and mashup songs like in Shrek. Majorie, you make it more easy to leave because I know my research project is in good hands. Good luck!

A very special thank you goes out to Iris and Lieke for always being honest with me, especially when I was being too hard on myself. The intervention banner was a good threat during the year and I am grateful that you are my roommates and friends.

Aline and Jildou, thank you for always being there for me. Finally, I would like to thank my parents for always believing in me. I feel so grateful and blessed to have parents like you.

Marije van der Vee
October 2018

Contents

Preface	v
List of acronyms	ix
0 Introduction	1
1 Clinical background	3
1.1 Peripheral arterial disease	3
1.2 Symptoms	3
1.3 Pathophysiology	4
1.4 Diagnosis	5
1.5 Treatment	6
1.6 Aim of study	7
2 Introduction to echoPIV	9
2.1 Medical ultrasound	9
2.2 High frame rate imaging	10
2.3 Microbubble contrast agents	10
2.4 EchoPIV	12
2.5 Visualisation of UCA	13
2.6 Post-processing of US images	14
3 Ultrasound settings	17
3.1 US transducer choice	17
3.2 Transducer settings	21
3.3 Verasonics US sequences and in vitro testing	23
4 Safety measurements	31
4.1 US output parameters	31
4.2 Thermal measurements	37
5 Study protocol	41
5.1 Introduction	41
5.2 Objectives	41
5.3 Study design	42
5.4 Study population	42
5.5 Methods	43
6 In vivo echoPIV - preliminary results	45
6.1 Introduction	45
6.2 Methods	45
6.3 Results	48
6.4 Discussion	54

6.5 Conclusion	57
7 Conclusions	59
References	61
8 Appendix A; Study approval letters	69

List of acronyms

AM	Amplitude modulation
CBR	Contrast-to-background ratio
CCMO	Central Committee on Research Involving Human Subjects
CEUS	Contrast enhanced ultrasound
CFA	Common femoral artery
CFD	Computational fluid dynamics
CI	Intermittent claudication
CTA	Computed tomography angiography
CTR	Cyst-to-tissue ratio
DCB	Drug coated balloon
echoPIV	Echo particle image velocimetry
FDA	Food and Drug Administration
fps	Frames per second
GCP	Good Clinical Practice
GUI	Graphical user interface
HFR	High frame rate
IEC	International Electrotechnical Commission
Isppa	Spatial-peak pulse-average Intensity
Ispta	Spatial-peak time-average Intensity
MI	Mechanical index
MRA	Magnetic resonance angiography
OSI	Oscillatory shear index
PAD	Peripheral arterial disease
PFA	Profunda femoral artery
PI	Pulse inversion
PII	Pulse intensity integral
PIV	Particle image velocimetry
PRF	Pulse repetition frequency
PSV	Peak systolic velocity
PTA	Percutaneous transluminal angioplasty
PVA	Polyvinyl alcohol
PW	Plane wave
SFA	Superficial femoral artery
SVD	Singular value decomposition
UCA	Ultrasound contrast agents
US	Ultrasound
WSS	Wall shear stress

Introduction

The prevalence of patients with peripheral arterial disease (PAD) in the lower extremity is rising. In ten years the number of patients has increased by nearly 25% to approximately 202 million people, of whom 40,5 million are European inhabitants.¹ When supervised exercise therapy is unsuccessful as treatment and the complaints are disabling, revascularisation is considered. The current guidelines advocate endovascular treatment in all femoro-popliteal lesions with a total length of <25 cm.² Although there has been a rapid progress in the field of endovascular therapy, in-stent restenosis in the lower extremity remains a major challenge.³⁻⁵ Unfortunately, it is currently not possible to predict disease progression or whether a patient is more prone to in-stent restenosis and requires additional treatment.

PAD is a systemic disease caused by atherosclerosis, a slow process where the artery narrows due to plaque formation. Arterial branches, such as the femoral bifurcation, are more prone to atherosclerosis.⁶ It has been suggested that blood flow dynamics are involved in the localisation and the initiation of atherogenesis. Disturbances in arterial blood flow are known to modify the response to endothelial injury.⁷ Moreover, atherogenesis and the formation and progression of atherosclerotic plaques are suggested to be locally stimulated by low velocities close to the vessel wall.^{8,9} This implies that blood flow dynamics are involved in the localisation and the initiation of atherogenesis, and might be of predictive value.

In vivo blood flow quantification might contribute to an explanation of atherosclerotic disease progression. Linking flow derived parameters with disease progression could allow to predict whether a patient is more prone to in-stent restenosis. High frame rate contrast-enhanced ultrasound (HFR-CEUS) velocimetry is a recent development in the quantification of human blood flow. Feasibility of echo particle image velocimetry, echoPIV, has been shown in healthy volunteers in the carotid artery and the abdominal aorta.¹⁰⁻¹² Before echoPIV can contribute to an explanation of femoral in-stent restenosis, its feasibility around stents in PAD patients must be shown. Therefore the aim of this study is to determine the feasibility of blood flow quantification with echoPIV, near stented lesions in the femoral artery.

The work that is done in preparation of the feasibility study can be read in this thesis that is composed of 7 themed chapters. The **first chapter** gives a brief overview of the clinical background and will address more comprehensively the aim of the study. The **second chapter** highlights the key theoretical concepts of echoPIV. Technical considerations regarding the transducer and ultrasound (US) settings that will be applied in the feasibility study are discussed in **chapter 3**. The US

research devices that have been used in the study do not have the appropriate CE marking for clinical use. **Chapter 4** elaborates the measurements that have been performed to ensure patient safety.

The feasibility study is conducted according to a study protocol, which is elaborated in **chapter 5**. The Central Committee on Research Involving Human Subjects (CCMO) and the institutional review board of Rijnstate hospital approved this protocol. The approval letters can be found in the appendix. So far, one patient has participated in the study. First insights, and recommendations for further conducting the patient study will be discussed in **chapter 6**. The **final chapter** summarises the main findings of this project and draws an overall conclusion.

Clinical background

1.1 Peripheral arterial disease

PAD is a medical condition where blood flow to- and oxygenation of tissue is compromised as a result of a stenosis or occlusion of the arteries, mostly due to atherosclerosis. Atherosclerosis is frequently observed in the bifurcation of the common femoral artery (CFA) in patients with PAD.^{13–16} This artery is of great importance in lower extremity PAD because it provides the main arterial blood supply to the lower limb, as can be seen in figure 1.1. The CFA is the continuation of the external iliac artery after passing the inguinal ligament. The CFA bifurcates into the superficial femoral artery (SFA) and the profunda femoral artery (PFA), also called deep femoral artery. The SFA continues as the popliteal artery and the PFA branches again into the medial circumflex femoral artery and the lateral circumflex femoral artery.

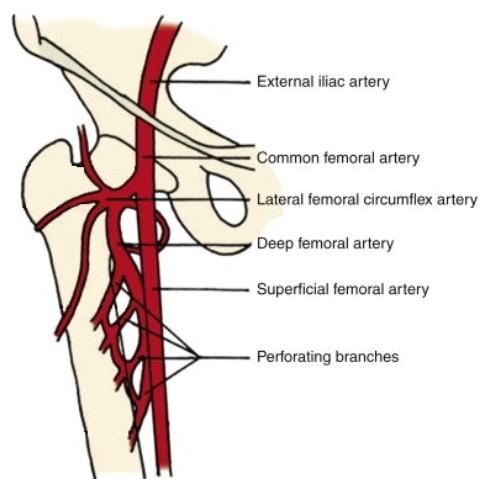


Figure 1.1: Femoral artery and its major branches.

The SFA continues as the popliteal artery and the PFA branches again into the medial circumflex femoral artery and the lateral circumflex femoral artery.

Several risk factors have been identified for PAD. They are identical to the risk factors for atherosclerosis in general, due to the pathophysiology of PAD. Diabetes Mellitus, dyslipidaemia, hypertension and smoking are all strongly associated with an elevated risk of PAD. Age and gender are also important determinants, the prevalence of PAD rises with age and symptomatic PAD is more common in men.^{2,17}

1.2 Symptoms

The majority of the patients with PAD are asymptomatic. Intermittent claudication (CI) is the earliest and the most frequently seen symptom in lower extremity PAD. About 6.5% of the patients with PAD in the Netherlands have intermittent claudication.^{18,19} Patients may complain about aching or burning pain, heaviness, or tightness in the muscles of their legs that usually begins after a period of exercise and diminishes or goes away after a moment of rest. In the later stages of lower extremity PAD, patients may develop rest pain or ischemic ulceration and gangrenous necrosis as a progression of

Fontaine classification		Rutherford classification			
Stage	Symptoms		Grade	Category	Symptoms
I	Asymptomatic	⇔	0	0	Asymptomatic
IIa	Non-disabling CI		I	1	Mild CI
		⇔	I	2	Moderate CI
IIb	Disabling CI		I	3	Severe CI
III	Ischemic rest pain	⇔	II	4	Ischemic rest pain
IV	Ulceration or gangrene		III	5	Minor tissue loss
		⇔	III	6	Major tissue loss

Table 1.1: Clinical stages of PAD.²

tissue hypoperfusion that may eventually require amputation.^{2,13–15} The clinical stages of PAD can be categorised by either the Fontaine classification which is commonly used in the Netherlands, or the Rutherford scale that is more common in other countries. The stages are listed in table 1.1.²

1.3 Pathophysiology

The pathogenesis of PAD can best be explained through a study of atherogenesis in general. Atherogenesis refers to the developmental process of atheromatous plaques that arise as a result of a chronic disease of the arterial wall called atherosclerosis. Atherogenesis can be subdivided into three stages. The first phase involves adhesion of leukocytes on the inner arterial wall due to the expression of adhesion molecules by the endothelial cells.^{13,20} Endothelial activation and the expression of adhesion molecules can be provoked by hypertension, hyperlipidemia, pro-inflammatory mediators, changes in endothelial permeability, perturbations in local hemodynamics or abnormal shear stress.^{20–24} After the migration of leukocytes into the intima they mature into macrophages and accumulate lipids which give them a foamy appearance. Meanwhile, the recognisable stage of atherosclerosis, the fatty streak, is formed by foam cells.^{13,20} The second phase involves lesion progression where vascular smooth muscle cells migrate into the intima where they proliferate and form atherosclerotic plaques. This process involves the production of extracellular matrix molecules such as collagen and elastin by the smooth muscle cells.^{13,20} The accumulation of cellular debris and extracellular lipids creates a necrotic core within the plaque because of inefficient clearance of dead cells.²⁵ Tissue ischemia can be a result of the plaque that induces flow limitations to the distal vessels. In the last phase, potential disruption of the plaque causes interaction between blood and procoagulant material from the fibrous cap, triggering thrombosis. Subsequently, a thrombus could lead to interruption of blood flow locally or embolize and cause a distal occlusion.^{13,20}

Atherosclerosis is typically localised at sites with complex or disturbed blood flow patterns, e.g. at arterial branches such as the femoral bifurcation. Disturbed hemodynamic patterns can include blood flow recirculation or reversal, and is known to modify the response to endothelial injury.^{6,7} Vascular endothelial cells experience shear stresses induced by the friction of the blood on the vessel wall. The wall shear stress (WSS) is defined by the tangential stress that arises from the friction of the blood on the vessel wall. The blood flow velocity and the arterial geometry, e.g. an obstruction, are important determinants for the WSS.⁹ Blood recirculation disturbs the flow field that no longer runs parallel to the vessel wall. This causes the WSS to become low and/or oscillatory which is associated with the development of atherosclerotic plaques. A number of atherogenic genes in endothelial cells

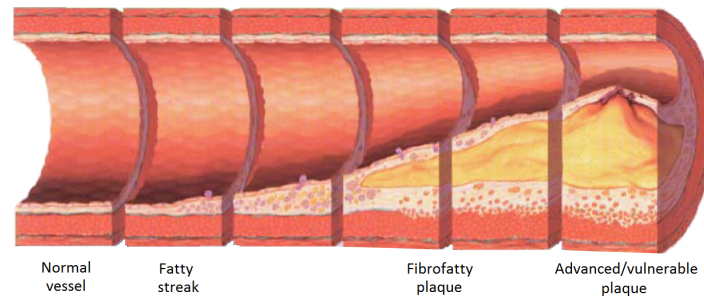


Figure 1.2: Stages in the development of atherosclerotic lesions. Adapted from N.D. Patchett.

are activated in response to the disturbed flow patterns and WSS.^{6,8} It has been shown that cell proliferation is induced in response to low WSS and that oscillatory WSS induces leukocyte adhesion which is seen as the initial step in atherosclerosis. Moreover, shear stresses induced by laminar flows are associated with protective effects due to down regulation of atherogenic genes.^{6,7} In response to a high WSS, vascular endothelial cells align with each other in an elongated pattern while the morphology becomes non-organised when they are exposed to low WSS.^{6,7} Normally, the cell junctions in the organised endothelial intima enable the passage of macromolecules. An increase in permeability to lipoproteins is likely caused by the disruption of the cell junctions due to this random morphology.⁶ The formation and progression of an already formed atherosclerotic plaque is subsequently locally stimulated by disturbed flow patterns and low shear stresses.⁹

1.4 Diagnosis

PAD can be recognised by several symptoms. Absence of peripheral pulsations, changes in colour and temperature of the feet and wounds that heal slowly are commonly seen symptoms. A plaque rupture can cause acute thrombosis which can result in acute ischemia. It is important to differentiate PAD from acute ischemia in order to choose the right treatment; the latter can also have other causes like a peripheral thromboembolism as a result of atrial fibrillation.

The diagnosis of PAD is confirmed by determining the ankle-brachial pressure index (ABI). To obtain the ABI, systolic blood pressure is determined in the posterior tibial artery and dorsalis pedis artery using a blood pressure cuff that is placed above the ankle and a Doppler instrument. The ABI is calculated for each side of the body by dividing the highest measured pressure in the foot by the systolic brachial pressure in either arm. In a healthy subject (good arterial leg circulation) the ABI at rest is around 1. An ABI value of <0.9 is usually taken as a pathological indicator of PAD.²⁶

In addition to the ABI determination at rest, there are multiple diagnostic modalities available for planning an intervention. Duplex ultrasound can be used to localise and quantify atherosclerotic lesions. Additionally, the velocity of the blood can be determined in the affected blood vessel using Duplex scanning. The difference in peak systolic velocity (PSV) measured proximal or distal to the stenosis versus the PSV in the stenosis can provide information about the severity of the lesion. The hemodynamic significance of the stenosis provided by the PSV ratio is however limited.²⁷ Computed tomography angiography (CTA) or magnetic resonance angiography (MRA) gives the most reliable anatomic information about lesions in a blood vessel. According to the results of the CTA or MRA it can be determined whether the patient is eligible for percutaneous transluminal angioplasty (PTA) with or without stenting, or surgery.²⁸

1.5 Treatment

Besides the treatment of lower PAD, secondary risk prevention focusing on atherosclerosis is provided because of an increased risk of cardiovascular events.² Smoking cessation, a balanced diet and regular physical exercise is recommended. Antithrombotic drugs, in particular platelet aggregation inhibitors, and medication for hypertension and dyslipidemia should be used in order to reduce the risk of an event.^{29,30}

Exercise therapy is used as initial therapy approach in patients with PAD. It may reduce symptoms, increase the maximum and pain-free walking distance, improve the quality of life and mostly it is effective to delay or avoid intervention.² Revascularisation is considered in patients with tissue necrosis, pain at rest or when a (supervised) exercise therapy was unsuccessful and the complaints are lifestyle-limiting or disabling.

During the last decades there has been a shift towards endovascular treatment, also for the more severe lesions. In case of complex femoropopliteal occlusive disease, an open venous femoropopliteal bypass was the principal strategy for a long time. Restoration of blood flow by endovascular procedures, e.g. PTA with or without stenting, has proven to be an attractive alternative to open surgical procedures because of its less invasive character. Innovations in the field of endovascular therapy has led to a change in the guidelines. The current version of the ESVS guidelines advocate endovascular treatment in all femoro-popliteal lesions with a total length of 25 cm or shorter.² Numerous factors, e.g. severity and the location of the lesion, patient condition or the availability of autologous conduit, need to be taken into account prior to treatment decision. Regardless of the chosen strategy, an (unsatisfying) adequate inflow is required to succeed the revascularisation.^{31,32}

PTA is nowadays considered for relatively simple and short lesions (<3 cm). Although PTA offers good results in short lesions, restenosis occurs frequently in more extensive lesions.³³ Therefore, stenting, using self-expanding nitinol stents, is often performed because of decreased restenosis rates after primary implantation and improved long-term patency in intermediate lesions^{34,35} Still, restenosis rates after 2 years were unsatisfying (45,7%) and shows that stent development is required to address the predominant cause of stent failure.³⁵ An increased length and complexity of the lesion is correlated with higher failure rates.^{36,37}

There are multiple innovations to reduce intimal neo-hyperplasia and in-stent restenosis. Drugs, particularly paclitaxel, have been added to balloons (drug coated balloons, DCB) and stents (drug eluting stents). DCB angioplasty showed an increased primary patency after 24 months compared to a standard PTA (78.9 % vs. 50.1%).^{38,39} Also, drug eluting stents show better long term results compared to bare metal stents, with a 5-year primary patency rate of 66% and 43% respectively.⁴⁰ Furthermore, an expanded lining has been added to a nitinol stent frame creating a covered stent to reduce intimal hyperplasia. A heparin-bonded covered stent showed an increased 2-year patency rate when compared to a bare metal stent in long SFA lesions.⁴¹ Stent graft patency is however limited by the development of intimal hyperplastic edge stenosis. When edge stenosis occurs, more than 50% of the lesions develop at the proximal edge and 35% develop both distal and proximal.⁴²

If the lesion is >25 cm, endovascular approach is still possible, but femoro-popliteal bypass achieves better long-term patency.² Especially when using the saphenous vein, which shows a superior patency compared to other grafts and conduits.^{43,44} A heparin-bonded covered stent also showed

promising results for long segment lesions. Similar patency rates were seen in the comparison with a femoropopliteal bypass, both prosthetic and venous conduit,^{45,46} while there was less morbidity, faster recovery and an improvement in health status at 1 year after implementation.⁴⁶

The last mentioned multicentre randomised controlled trial, also suggested that a concomitant endarterectomy of the CFA, regardless of an endovascular or surgical approach, might be a predictor for success.⁴⁶ These findings confirm the large impact of significant changes in the arterial geometry in the development of atherosclerosis. Even though there were no stenotic lesions proximal to the bypass or stent in the SFA, it seems that the hemodynamic environment of the CFA might have impacted the outcome. The removal of a plaque could positively influence the flow characteristics at the inflow section of the stent or bypass.

1.6 Aim of study

As mentioned in the previous section, endovascular approach has become the principal strategy in the surgical treatment of femoropopliteal occlusive disease, and mostly replaced the invasive open procedures.² Although long-term patency has been increased over the years, in-stent restenosis is still the predominant cause of stent failure.³⁵ Especially, the edges of endografts are prone for restenosis.⁴² It is well known that the response to endothelial injury is modified by changes in blood flow and WSS.^{6,7} Atherogenesis and the formation and progression of atherosclerotic plaques are locally stimulated by a low or oscillatory WSS.^{6,8,9} The placement of rigid frameworks induces significant changes in arterial geometry and thereby in the hemodynamic environment and WSS.⁸

Yet, it is a clinical challenge to predict atherosclerotic disease progression and identify the patients at highest risk for restenosis. Knowing that local blood flow has a significant influence on the development of atherosclerosis and therefore potentially on stent patency, the question arises if flow derived parameters could predict disease progression or in-stent restenosis. In-stent characterisation of blood flow could identify disturbed flow patterns and low or oscillatory WSS regions. If flow-derived parameters could be linked to disease progression, it might enable the recognition, prediction and explanation of (in-stent) restenosis. Subsequently, individual patients or specific stented lesions could be identified that are more prone to disease progression and subsequent the development of restenosis.

Identification of disease progression in individual patients could radically improve health care outcomes. It could help vascular surgeons to make a well-considered choice regarding treatment, e.g. to perform a concomitant endarterectomy. It could help to understand which patients, or which arterial lesions and geometries, would derive the greatest benefit from innovations like DCBs and drug coated stents. Next to that, it could lead to an improved design of stents. Ultimately, this information should contribute to an improved patency with a lower re-intervention rate and thus a better clinical outcome for the patient.

A previous study performed by our group showed the feasibility of echoPIV in the aortic bifurcation in healthy volunteers. Through the use of HFR-CEUS local flow patterns could be quantified.¹² Before this technique can be used around stents in the femoral artery, feasibility must be shown. Therefore the aim of this study is to determine the feasibility of femoral blood flow quantification near stented lesions in the SFA using echoPIV.

Introduction to echoPIV

The visualisation and quantification of real-time blood flow phenomena in humans is still a challenge. Although blood flow can be studied with 4D flow magnetic resonance imaging (MRI), it has several drawbacks. Metal stents can cause disturbances in the magnetic field and there is a trade-off between the temporal resolution and the spatial resolution.⁴⁷ Next to that, MRI is an expensive method that requires relatively long scanning times and comes with significant waiting times when there is no emergency setting. In the clinical practice, US techniques are regularly used to obtain information about geometry of the vessels, possible lesions or the velocity of the bloodstream. Current clinical US techniques are low in cost and can be applied quickly and easily. They lack however the ability to recognise motion details or to perform quantitative flow measurements because of frame rate restriction.^{48–51} This chapter will review the current US techniques and discuss how US can be used in quantifying flow phenomena.

2.1 Medical ultrasound

In ultrasound imaging an US pulse is transmitted into the body that partially reflects on tissue interfaces, and is scattered through irregularities in tissue. The amplitude of the recorded echo provides information about the acoustic impedance of tissue and the return time gives information about the depth of the reflecting surface because there is little variation in the speed of sound in human tissue. Compared to other medical imaging techniques, US imaging has multiple advantages. Besides low costs, US provides real time capabilities and does not use harmful ionising radiation.⁴⁸

US array transducers consist of multiple piezoelectric elements. By applying an alternating voltage, the elements start to oscillate producing ultrasonic pressure waves. Vice versa, by imposing a pressure wave on the elements they produce an electronic voltage. A transducer array consists of several elements that can transmit and receive pressure waves and electric signals independently. The geometry of a transducer and the transmit waveform, in particular its delay, determine the beam pattern of a transducer.^{48,49}

Conventional beam forming or B-mode is based on a pulse-echo technique. Sequential US pulses are emitted to create a focus at a chosen depth. A consecutive pulse is sent by an element when the previous one is received by the transducer. Each pulse and its backscattered echoes contribute to one image line. The frame rate is therefore limited by the number of lines per image. The frame rate can either be improved by decreasing the number of lines or by shortening the pulse repetition time and image less deep. A higher frequency also decreases penetration depth although it increases

axial resolution. The lateral resolution can be increased by narrowing the ultrasound beam. There thus exists a compromise between temporal resolution, spatial resolution and the field-of-view. To recognise motion details, HFR imaging is desired. For analysing fast flow profiles the frame rate that comes with conventional US is insufficient due to low temporal resolution.^{48–51}

Colour-Doppler is the most used method to determine the blood flow velocity in the clinical practice. It provides information about the direction of flow. This US technique is often combined with grayscale images obtained by conventional ultrasound scanning, called Duplex US. Subsequently, Colour-Doppler is limited by a low frame rate and thus low temporal resolution. Next to that, only the velocity component in the direction of the beam can be obtained. It is hard to align the axis of the beam with the flow direction in complex geometries like a bifurcation. Besides, to estimate velocities it is assumed that the blood flow is unidirectional and aligned with the vessel wall.^{49,52} Therefore, Duplex US can not be used as an accurate tool to perform quantitative flow measurements. Vascular sonographers use Duplex US only to identify stenotic lesions and to obtain to some extent insight in the local hemodynamics. A newer US based technique to quantify flow patterns uses transverse oscillations, to detect Doppler shifts in two directions. However, depth is limited and therefore this method is not currently feasible in the femoral bifurcation.^{51,53–55}

2.2 High frame rate imaging

Frame rate is an important feature in blood flow quantification in order to recognise motion details. Therefore, several techniques are conceived using HFR imaging.^{49,50} The physical optimum is plane wave (PW) imaging where all transducer elements are excited simultaneously. One full image is constructed per transmit at the expense of the spatial, mainly lateral, resolution. PW compounding can be used to increase the lateral resolution, several tilted plane waves from different angles can be excited and summed up to construct one image. A higher amount of angles decreases the temporal resolution but increases the spatial resolution significantly. The time required to obtain an image of the same quality as in conventional US is 5-10 times faster. Consequently the frame rate can be increased by the same amount without lowering the spatial resolution compared to conventional US.^{48,50,56,57}

2.3 Microbubble contrast agents

Microbubble ultrasound contrast agents (UCA) have a diameter of 1-10 μm and are composed of bio-compatible materials. They can be used to increase echogenicity. Microbubbles exhibit resonance at typical diagnostic US frequencies (around 3 MHz).⁵⁸

The increased echogenicity is mainly caused by the volumetric oscillation of the UCA. Insonated microbubbles contract and expand their diameter several-fold. Next to that, because of the large difference in acoustic impedance between blood and a bubble filled with gas the latter scatters much more strongly. The signals generated by the microbubbles are US dependent. At low acoustic power, microbubbles behave linearly and re-emit signals with the same frequency content as the excitation US pulse. Non-linear vibrations occur when the acoustic power is increased. When hit by an ultrasound wave, a bubble expands more in diameter in response to a pressure drop compared to compression during pressure rise. This non-linear response is illustrated in figure 2.1. The asymmetric movements cause asymmetric sound reflections that hold the fundamental or transmitted frequency

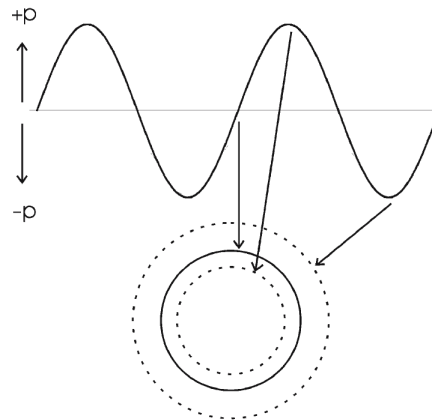


Figure 2.1: Simplified model of the non-linear response of the microbubble to the pressure rise and -drop of the ultrasound wave.⁵⁸

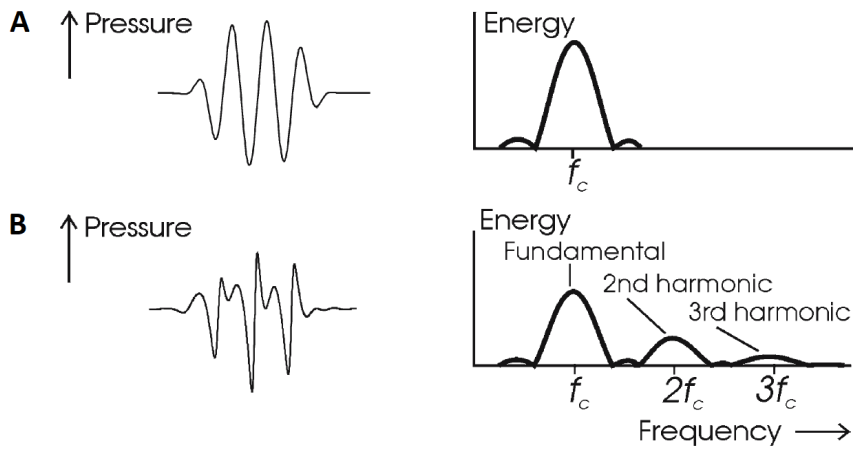


Figure 2.2: **A)** US signal with a transmitting central frequency (f_c) and a linear frequency response. **B)** Non-linear re-
flected wave from a microbubble and its (harmonic) frequency response. Adapted from M. Averkiou and E. Quiaia^{58,59}

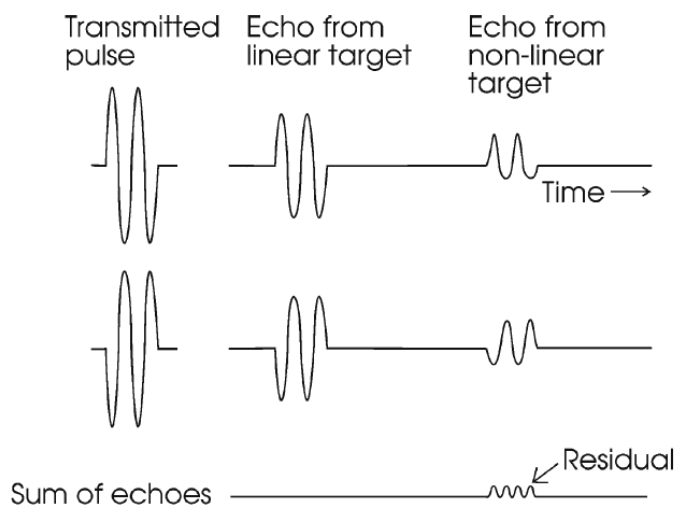


Figure 2.3: Pulse inversion imaging involves summing the echos from a non-inverted and inverted pulse. This results in cancelling out the linear signals en preserve the non-linear signals from e.g. microbubbles.⁵⁸

(f_0), multiple harmonic ($2 \cdot f_0$, $3 \cdot f_0$, $4 \cdot f_0$, etc), and subharmonic ($f_0/2$, $f_0/3$, etc) frequencies.^{60,61} This is intrinsically different than the scattering from tissue that is considered to be linear. The difference in signal and frequency response can be seen in figure 2.2. If the acoustic power is further increased, the expansion causes bubble shell disruption and eventually bubble destruction. Besides the acoustic power, long US pulses and a low transmitting frequency increase the probability of destroying microbubbles. Both sub- and higher harmonic frequencies are emitted when microbubbles destruct.⁵⁸

In order to detect microbubbles in the vascular system, they should be intravenously injectable and have a high stability passing by the pulmonary and cardiac circulation into the peripheral bloodstream. Next to that, they should be inert, distribute equally and provide a long enough duration so measurements can be performed. A low Stokes number is required because it is of great importance that the bubbles follow the bloodstream precisely. It is also important that the contrast bubbles are not too susceptible to US waves to prevent immediate destruction. Stability can be increased by encapsulation and by selecting a filling gas with a low diffusivity.^{58,62}

In general, microbubbles have an excellent safety profile with a low incidence of side effects that are of mild intensity and transient.^{58,62,63} A transient alteration in taste or experiencing a facial sensation of warmth, an unpleasant sensation or local pain at the site of injection is most frequently seen. Individual cases include chest pain, headache, nausea and shortness of breath.⁶³ Microbubbles in the vascular system can increase the incidence of US bio effects through several acoustic mechanisms. The oscillation of bubbles can result in local heat production and microstreaming around the bubble and localised shear stresses. An higher acoustic power can cause the bubble to collapse and aggravate previous mentioned effects. These effects, however, occur on a microscale and are localised and transient.^{58,64}

Sonovue

SonoVue is a sulphur hexafluoride-filled (SF₆) microbubble UCA encapsulated by a flexible phospholipid shell that is prepared as a lyophilisate powder. This microbubble has two main advantages compared to air-filled microbubbles. First, the low solubility of the gas and the shell stabilisation by the phospholipids, that reduce the surface tension, provide a high and prolonged stability in the human body.⁶⁵ Sulphur hexafluoride is an inert gas that is eliminated by the lungs after a few minutes. The phospholipid shell is filtered by the kidneys and eliminated by the liver.⁵⁸ The mean diameter is 2.5 μm , while 90 % of the bubbles are smaller than 6 μm .⁶⁶

2.4 EchoPIV

Particle image velocimetry (PIV) is a method to obtain quantitative flow information. Flow dynamics can be visualised by seeding particles in the flow. In vitro, these particles are fluorescent and can be visualised by shining a laser beam onto the fluid, in synchronisation with a high-speed camera. In vivo the laser beam and camera can be replaced by HFR ultrasound imaging and microbubble contrast can be used as seeding particles. The ultrasound images are analysed to determine the distances travelled by particles between two frames. Images are evaluated through a pairwise cross-correlation of multiple sub-images (interrogation areas) in all frames.⁶⁷ Next, a velocity field can be calculated from the distance that particles have travelled within the time frame of two consecutive images.^{68,69}

In several studies it is shown that echoPIV is a reliable method to quantify flow patterns in-vitro. Velocity vectors and calculation of the WSS can be obtained accurately. In vitro the results can be validated by comparing it with computational fluid dynamics (CFD) results⁷⁰ or with laser-PIV.^{10,71}

The combination of HFR and UCA offer new possibilities as a fast and easy technique to determine blood flow in vivo.⁷² The quantification of blood flow in humans by echoPIV is a recent development. In the heart, left ventricular flow patterns have been visualised and quantified using echoPIV.⁷³ In vivo validation studies performed on the carotid artery showed good agreement in comparison with 4D-MRI scans.^{10,11} Also in the abdominal aorta, echoPIV proved to be feasible to quantify blood flow patterns.¹² These validation studies were performed on a limited number of healthy subjects.

2.5 Visualisation of UCA

The increase in echogenicity by the microbubbles is visualised in conventional imaging.⁷⁴ There are multiple techniques that take advantage of the specific properties of microbubbles contrast agents, that are discussed in section 2.3. Harmonic imaging exploits the non-linear behaviour of microbubbles. The US image is made from the 2nd harmonic ($2 \cdot f_0$) while the fundamental component (f_0) is removed by filtering. Because tissue is less non-linear than UCA, the filtering causes tissue suppression in the image. However, there is a trade-off between imaging resolution and contrast detectability due to the spectral overlap between fundamental and the harmonic component. Separation of the harmonic content can be eased by narrowing the transmit bandwidth of the transducer at the cost of spatial resolution.^{59,74} Next to that, sensitivity is sacrificed because most of the scatter from both UCA and tissue falls within the fundamental part of the spectrum.⁵⁸

Multipulse techniques such as amplitude modulation (AM) and pulse inversion (PI) have been developed to suppress tissue through signal separation without decreasing the spatial resolution. Instead, these imaging modalities make use of subtraction rather than filtering.⁷⁵ PI makes use of two transmitting pulses of which the second pulse is the inverse of the first waveform. The echoes from the non-inverted and inverted pulse are summed up to create one acquisition. Tissue scattering is considered to be (mainly) linear and will therefore be cancelled out in the summed echo causing tissue suppression in the reconstructed image. Non-linear responses, from e.g. microbubbles, will form a residual signal in the summed echo as can be seen in fig. 2.3. The summed echo consists of the non-linear signals generated by the microbubbles.^{58,59,76} Amplitude modulation is a related technique to PI and varies the amplitude instead of the phase. An transmitted pulse with twice the amplitude of the previous one, causes an echo with approximately twice the amplitude from tissue. Microbubbles behave non-linearly to the different pulse amplitudes. Correction for the amplitude in the residual signal after subtraction leaves the non-linear behaviour of the UCA.⁵⁸

The main advantage of these multipulse techniques is that digital filtering is not required and echoes over the whole transducer bandwidth can be used to reconstruct an image.⁵⁸ Therefore resolution is superior as the fundamental part in an echo from a microbubble contains most energy,⁷⁴ as can be seen in figure 2.4. A carotid artery phantom was used for UCA visualisation and the ultrasound images can be compared of conventional imaging, harmonic imaging and PI. Although PI is superior, it has the disadvantage that it down-sizes the maximal achievable frame rate.

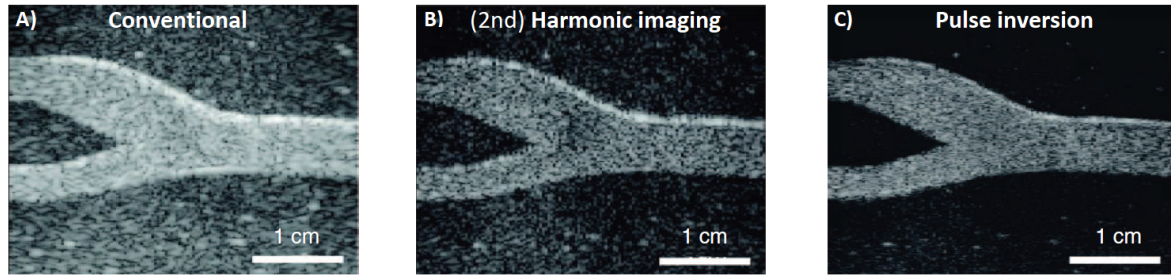


Figure 2.4: Visualisation of UCA in a carotid artery phantom by conventional imaging (A), (2nd) harmonic imaging (B) and pulse inversion (C). Tissue suppression and image resolution is superior in the PI image. Adapted from A. Stanzola.⁷⁵

2.6 Post-processing of US images

To overcome the frame rate limit in multipulse techniques, several post-processing techniques for HFR imaging are developed in order to enhance the bubble detectability and suppress the tissue. Many clutter filters are based on the supposed non-overlapping spectra between tissue and blood scatters.⁷⁷ This assumption is however not true for slow moving blood, e.g. due to a stenosis, and fast moving tissue due to a pulsating artery. The spectra of the last mentioned structures overlap. Singular value decomposition (SVD) filtering is a technique that is based on both the temporal and spatial differences between tissue and blood flow (with UCA).^{77,78} SVD processing has many applications in image processing and enables the suppression of moving tissue and the detection of slow moving UCA.

When SVD is applied on spatio-temporal cine data it exploits spatio-temporal correlation to decompose it into spatial and temporal patterns. Pixels reflecting moving tissue show low frequency variations in contrast with the rapid fluctuations caused by blood motion, both spatially and temporally. Therefore it can be said that tissue signal is more spatio-temporal coherent than flowing blood.^{77,78} Moreover, the intensities caused by tissue are typically higher than the intensities caused by blood motion. The difference in spatio-temporal coherence between tissue, flowing blood and bubbles, and noise is the basis in separation of the signals by SVD.^{77,78}

The first step is to reshape the RF data of all frames into one spatio-temporal representation, a Casorati matrix. The spatial data within one frame, lateral (n_x) and along depth (n_z), is stored in one column of Casorati matrix S .⁷⁷ The rows in matrix S represent the RF data for one pixel along time, and thus the total number of frames (n_t). The reorganisation of RF data and the factorisation of matrix S is visualised in figure 2.5. The SVD theorem states that matrix S can be rewritten into three matrices;⁷⁹

$$S = U \cdot \Sigma \cdot V^*, \quad (2.1)$$

where U and V are orthonormal, Σ is a diagonal matrix, and V^* stands for the conjugate transpose of matrix V . To factorise the matrices, the eigenvalues and eigenvectors of SS^* and S^*S must be calculated to fill in matrix U and V respectively. The square roots of the eigenvalues of SS^* are called singular values and make up the diagonal in Σ .⁷⁹

The spatial and temporal singular vectors of matrix S are reflected by the columns in matrix U and V^* respectively. The singular values in the rectangular diagonal matrix, Σ , are arranged in descending order and reflect the spatio-temporal coherence. Therefore, tissue movement is mainly described by

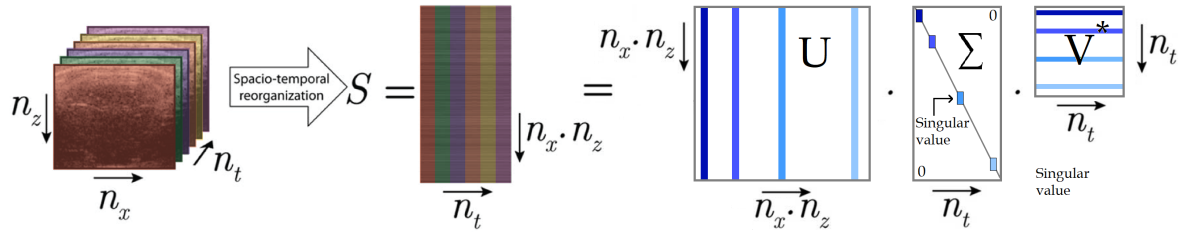


Figure 2.5: SVD illustration. US data is reshaped into a Casorati matrix (S) and factorised into three matrices, U , Σ and V^* . The degree of spatio-temporal coherence is described by the singular values in Σ and are arranged in descending order. Following, the high-rank singular values (dark blue) describe tissue, the medium-rank singular values describe blood and UCA and noise is described by the low-rank singular values. Adapted from C. Demené.⁷⁷

the first singular values and singular vectors (dark blue). Noise is the least spatio-temporally coherent and is therefore described by the last singular values and singular vectors (light blue). Flowing blood with UCA is represented by the values in between (medium blue). A new filtered matrix S , S^f , can be formed by rejecting the data that is described by the highest spatio-temporal coherence (tissue) and lowest spatio-temporal coherence (noise) singular values and singular vectors, leaving ideally only the echoes from flowing blood with microbubbles.^{77,78}

Ultrasound settings

Throughout this chapter the work that is done in preparation of a clinical patient study is elaborated. For this study, a (preclinical) Verasonics vantage 256 research US device (Verasonics Inc, Kirkland, US-WA) will be used. This device is previously used in patients, but does not have the appropriate CE marking for clinical use and has not been used in Rijnstate hospital so far. Before the Verasonics US device can be introduced in Rijnstate hospital, the patient study needs approval from an authorised institutional review board in the Netherlands and the institutional review board of Rijnstate hospital. The settings that emerge from this chapter will be used to write the study protocol which is required for study approval.

The first step in the process was to choose an appropriate ultrasound transducer (section 3.1). After this, ultrasound settings needed to be optimised in order to improve image quality (section 3.2). The transducer will be used for visualisation of the femoral artery and the UCA. In contrast to conventional commercial ultrasound systems, the beamforming, post-processing and reconstruction of ultrasound in the Verasonics is programmable and can be optimised for this project specifically. For script evaluation and testing, in vitro measurements were performed and discussed (section 3.3).

3.1 US transducer choice

Clinically, a linear transducer with a variable transmitting ultrasound frequency between 3-15 MHz is used in the peripheral vasculature of the lower extremity.^{56,80} The vascular sonographer, who will perform the in vivo measurements, is used to visualise the femoral artery with a linear probe of 3-9 MHz.

Three potentially suitable linear probes are available which are listed in table 3.1. Necessarily a probe is used that can receive a frequency that is twice the transmitting frequency (f_0). The second harmonics ($2 \cdot f_0$) results from the non-linear behaviour of the microbubbles.⁵⁸ For this reason is the L7-4v probe unfavourable. It can only receive frequencies properly up to 7 MHz. Therefore a comparison is only made between the L11-4v and the L12-3v transducer.

3.1.1 Methods

A tissue mimicking phantom (CIRS Model 040GSE, Norfolk, US-VA) designed to evaluate ultrasound transducers was used in the comparison. The phantom contains multiple grey scale targets and anechoic masses that can be used to analyse image quality.

	L7-4v	L11-4v	L12-3v
Frequency bandwidth (MHz)	4-7	4-11	3-12
Default center frequency (MHz)	5.208	6.250	7.813
Number of elements	128	128	192
Elevation focus (mm)	25	20	20

Table 3.1: Probe specifications.

As discussed in chapter 2, PW-US allows an essential increase in frame rate compared to conventional US that is required for tracking motion details in echoPIV (section 2.2). Therefore, several PW-US images were made with both probes in order to choose a probe. The center transmit frequency was varied between 4, 5 and 6 MHz. The total transducer aperture size of both probes is 38.4 mm.

Image quality is quantified by calculating the lateral resolution and a cyst-to-tissue ratio (CTR). The CTR is an alternative to signal-to-noise ratio. The effect of speckle can be quantified by determining the grey scale brightness level in a cyst object (signal) against a speckle background (noise). The squared average intensity within the cyst is compared to the squared average intensity of background tissue within the phantom, and determines the CTR. The grey scale targets on the vertical line at 10-80 mm depth are used to calculate the lateral resolution (figure 3.1). First, the pixel with the highest brightness level is detected in a 4 mm by 4 mm interrogation area around each target. The intensity of this pixel is compared to the relative intensity of the pixels laterally. The lateral resolution is defined as the width of the intensity peak at -6 dB.

3.1.2 Results

Two example images made by each probe can be seen in figure 3.1. In the right upper corner, two masses can be seen of which the left one is a hyper-echoic cyst and the right one is a more hypo-echoic cyst. Furthermore the grey scale targets are clearly visible. The brightness of the pixels that reflect the targets seems to be better in figure 3.1a, made by the L11-4 probe. The resolution seems however adequate in both figures.

The calculated lateral resolution of the L11-4v and the L12-3 probe at a central frequency of 4, 5 and 6 MHz can be seen in figure 3.2. The blue lines reflect the L11-4v transducer and the orange lines reflect the L12-3v transducer. Until a depth of 25 mm the L12-3v transducer shows a better lateral resolution. Up to a depth of 25 till 45 mm, the lateral resolution was fairly equal between the probes. From a depth of 45 mm, the L11-4v gave a better lateral resolution. The lateral resolution of the L11-4v seems to be more stable along the depth.

The calculated CTR can be seen in table 3.2. The ratios are categorised by the transducer, the hyperechoic and the more hypoechoic cyst, and the central frequency. The CTR calculations at the hyperechoic cyst are most relevant because the arisen signals here are most comparable to the high intensity signals that arise from the microbubbles. At a central frequency of 4 MHz, the L12-3v transducer gave the highest CTR. However at a central transmitting frequency of 5 and 6 MHz, the L11-4v transducer gave the highest CTR. Differences are however relatively small.

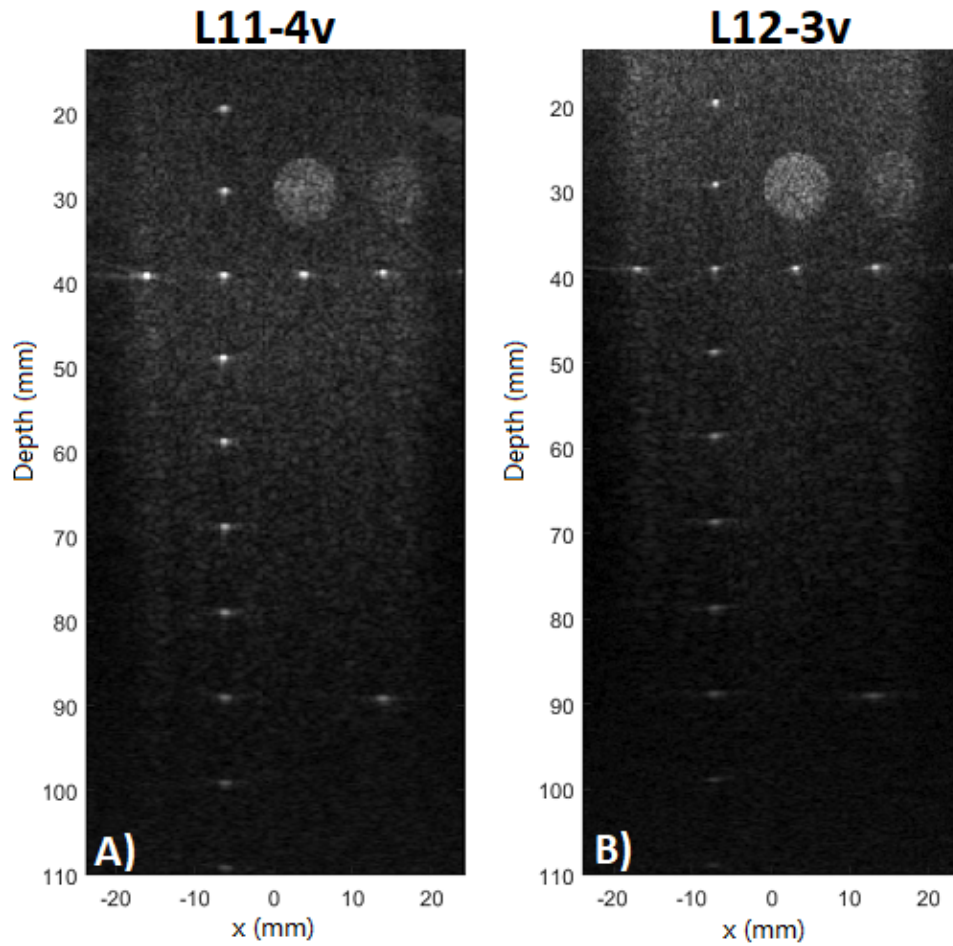


Figure 3.1: Images made by a L11-4v transducer (A) and a L12-3v transducer (B) using the tissue phantom (both $f_0 = 5\text{MHz}$).

	L11-4v		L12-3v	
	Hyperechoic	Hypoechoic	Hyperechoic	Hypoechoic
4 MHz	4.64	1.78	4.86	1.93
5 MHz	4.11	2.08	3.80	1.89
6 MHz	4.41	2.11	3.38	2.02

Table 3.2: CTR for the hyper- and hypo-echoic cyst of the L11-4v and the L12-3v transducer

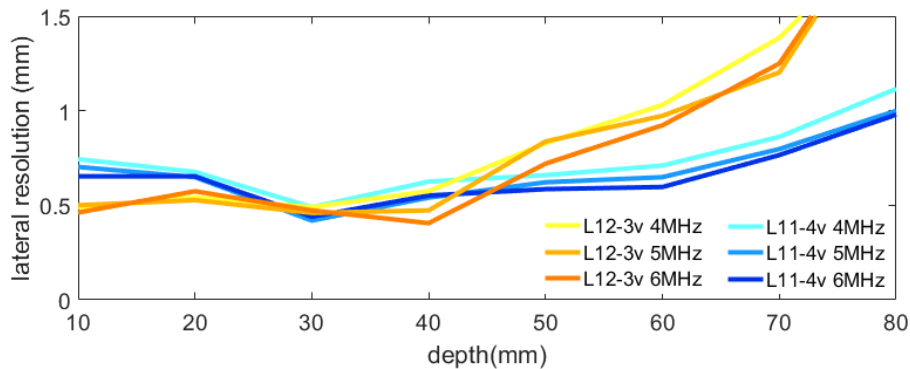


Figure 3.2: Lateral resolution at 10mm - 80mm of the L11-4v and the L12-3v transducer (4, 5 and 6 MHz).

3.1.3 Discussion

To choose the most optimal transducer for echo-PIV measurements at the bifurcation of the femoral artery it is important to consider the depth of the arteries. The CFA lies superficial under the skin at a depth of approximately 15 mm. The femoral bifurcation lies slightly deeper at a depth of circa 30 mm. In obese individuals this can be increased to 40-60 mm. According to the lateral resolution, the L12-3v should be the best option in thin patients and the L11-4v in bigger patients. The CTR does not give a clear indication to choose for a specific transducer.

The L12-3v probe has the disadvantage that it contains 192 elements. This is because only 128 of these elements can be used simultaneously. Subsequently, it limits the field of view significantly ($< 30\text{mm}$). Therefore an image was reconstructed from two acquisitions that was made up by 128 elements. The first aperture was made by the first 128 elements (1-128), while the second aperture was made by the last 128 elements (65-192). The reconstruction sums the data from the two acquisitions and computes intensity values to produce the full frame. This method increases the field of view, although it halves the maximal frame rate.

3.1.4 Conclusion

Overall, the image quality of both transducers is adequate to perform the echoPIV measurements. For practical reasons the L11-4v probe is chosen, because all the 128 elements of the transducer can be used simultaneously. This ensures a good field of view, does not limit the frame rate and does not complicate the Matlab scripts unnecessary.

3.2 Transducer settings

After choosing a probe, the echo transducer settings were selected. The goal was to find the most optimal transmit frequency and number of insonation angles for visualisation of the SonoVue microbubbles in the femoral artery by the L11-4v transducer.

3.2.1 Introduction

In figure 3.3a the power spectral density of SonoVue for low (dashed line) and high (solid line) acoustic power is depicted.⁵⁸ A clear peak can be seen around 3.5 MHz that represents the fundamental resonant frequency of the bubbles. To increase effective backscattering, the bubbles should be insonated by ultrasound with a central transmit frequency close to the resonant frequency. A second peak in power can be seen due to the 2nd harmonics. The frequency range of the L11-4v transducer is shown in figure 3.3b.⁸¹ The intensity of the signal decreases strongly above 12 MHz. It is therefore important to choose a transmit frequency below 6 MHz in order to receive the second harmonic. Furthermore, it can be seen that the intensity of the signal also strongly decreases below 4 MHz.

Studies have shown that a limited number of tilted plane waves can already increase image quality.^{57,82} Too many insonation angles can be destructive in the quantification of blood flow, because UCA motion at high speed becomes decorrelated because one frame includes more acquisitions which takes more time.^{82,83}

3.2.2 Method

The center frequency of the L11-4v probe was varied in five steps from 4 to 6 MHz. Image quality was quantified by calculating the lateral resolution, according to the method discussed in section 3.1. Based on the results and the properties of the SonoVue microbubbles and the L11-4v transducer, a central emitting frequency was chosen. Next, the number of insonation angles was varied between 1, 3, 5 and 21 angles. Image quality was again quantified by the lateral resolution.

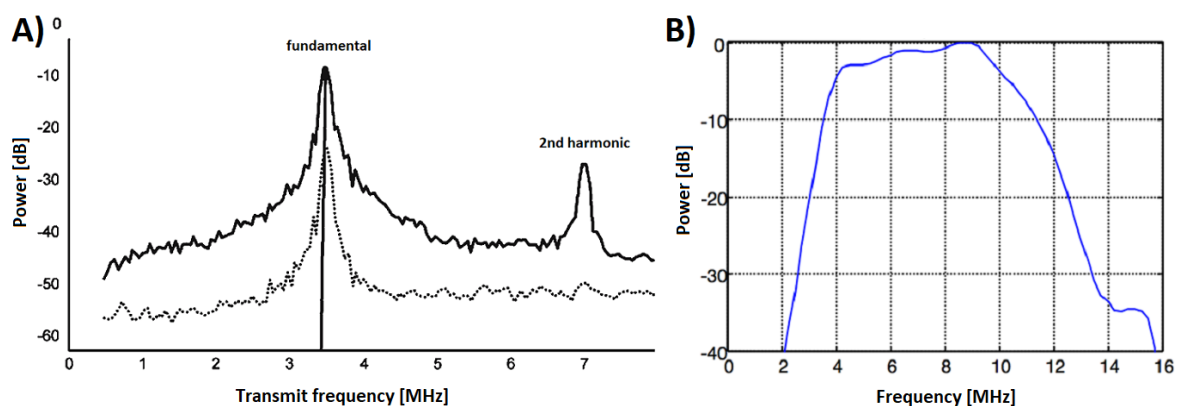


Figure 3.3: A) Power spectral density of SonoVue.⁵⁸

B) Frequency characteristics in emission of the L11-4v transducer.⁸¹

3.2.3 Results

In figure 3.4a, the lateral resolution can be seen for different center frequencies of the L11-4v transducer. The difference in lateral resolution is minimal. The fundamental resonant frequency and the frequency range of the transducer are therefore more decisive. The emitting frequency should be close to 3.5 MHz (resonant frequency). The L11-4v is most efficient between 4 and 10 MHz according to figure 3.4b. For this reason, a central emitting frequency of 4 MHz was chosen.

The lateral resolution for different insonation angles is depicted in 3.4b. An emitting frequency of 4 MHz was applied. It can be seen that a higher number of insonation angles improves the lateral resolution. No clear differences can however be seen in lateral resolution when 5 or 21 insonation angles are used. This implies that it is not necessary to increase the number of insonation angles above 5.

3.2.4 Conclusion

The findings in this section led to a central transmitting frequency of 4 MHz. Next to that, 3 angles of insonation will be applied in order to increase the lateral resolution, without compromising the maximal frame rate too much.

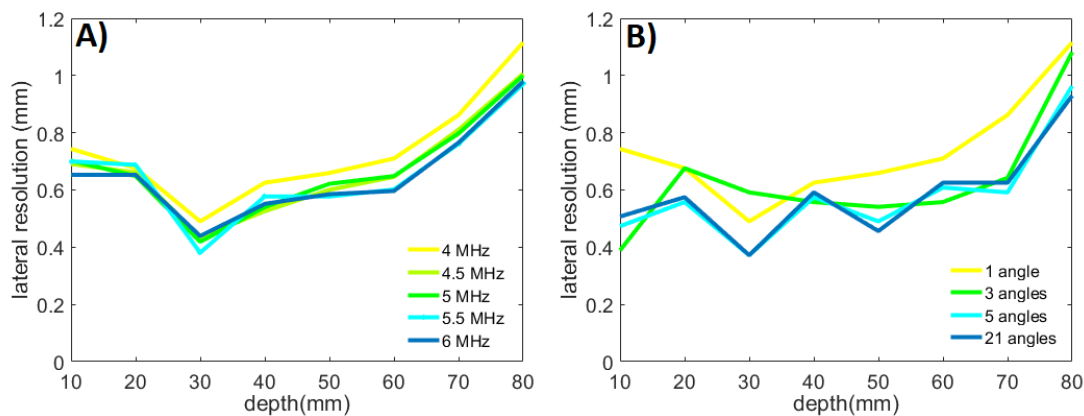


Figure 3.4: Lateral resolution at 10-80 mm of the L11-4v transducer at several frequencies (A), and at 4 MHz with multiple angles (B).

3.3 Verasonics US sequences and in vitro testing

This section discusses the testing and optimisation of the Verasonics imaging sequences using an in vitro flow phantom. The goal is to optimise the set-up and ultrasound settings to ensure repeatability of the in vivo echoPIV measurements. This is important because the patient measurements should be carried out as optimal as possible and be safe.

Prior to an in vivo HFR measurement, the vascular sonographer should be able to navigate to the region of interest in the femoral artery. This requires a real-time display of ultrasound images. Only then, anatomical landmarks can be used in the guidance to the region of interest. The vascular sonographer is used to optimise settings on the the clinical US machine while scanning the patient with the US transducer. This is not possible with a Verasonics US device which will be controlled by a researcher during the patient measurements. The vascular sonographer is only navigating with the US transducer. Still, it should be possible to adjust parameters like scan depth, the size of the aperture, the time gain control and the dynamic range during run-time. The researcher will execute these adjustments and obviously this demands effective communication between the researcher and the vascular sonographer.

Next to that, a real-time display is required to monitor the arrival and concentration of the Sonovue microbubbles in the femoral artery. Saturation of the UCA must be avoided to make the bubbles distinguishable, therefore the measurement should start after the first bolus has passed. On the other hand, the density of the bubbles should be sufficient to trace their motion and to give a proper reflection of the blood flow.⁸⁴ As soon as an equilibrium of UCA concentration is reached in the femoral artery, an echoPIV measurement will be performed. As discussed in chapter 2, PI can be applied to amplify the signals from the UCA and to eliminate much of the noise from the surrounding tissue (section 2.5). On top of PI, high-pass filtering can be applied to focus on the harmonic signals from the UCA which is expected to improve the visualisation of the microbubbles.

3.3.1 Methods

To generate the required imaging sequence, a script was written and executed in Matlab. The script defines several objects and thereby imaging parameters that are loaded into the Verasonics environment while executing. Two in-vitro measurements were performed in order to test and optimise the imaging sequences.

Flow phantom

An ultrasound phantom was made in order to test the Verasonics programming scripts. The phantom was made of polyvinyl alcohol (PVA, VWR International B.V., Amsterdam, the Netherlands), which possesses tissue mimicking properties when an appropriate ratio between PVA and water is chosen.^{85,86} To prevent crystallisation of water during the freeze-thaw cycles that are required for gelation, anti-freezing agents (e.g. ethylene glycol) can be added. This ensures homogenous mechanical properties of the phantom.^{85,86} In this model a commercially available vehicle coolant (Halfords Coolant Basic Safe -26 °C, Veenendaal, the Netherlands) was used to prevent crystallisation. The first step was to mix the cooling liquid with the PVA (10 wt%) until the PVA was dissolved. Hollow glass microspheres (Spherical 110P8, Potters Industries LLC, Melbourne, AUS-VIC) were added to the mixture to mimic ultrasound scattering (1 wt%).

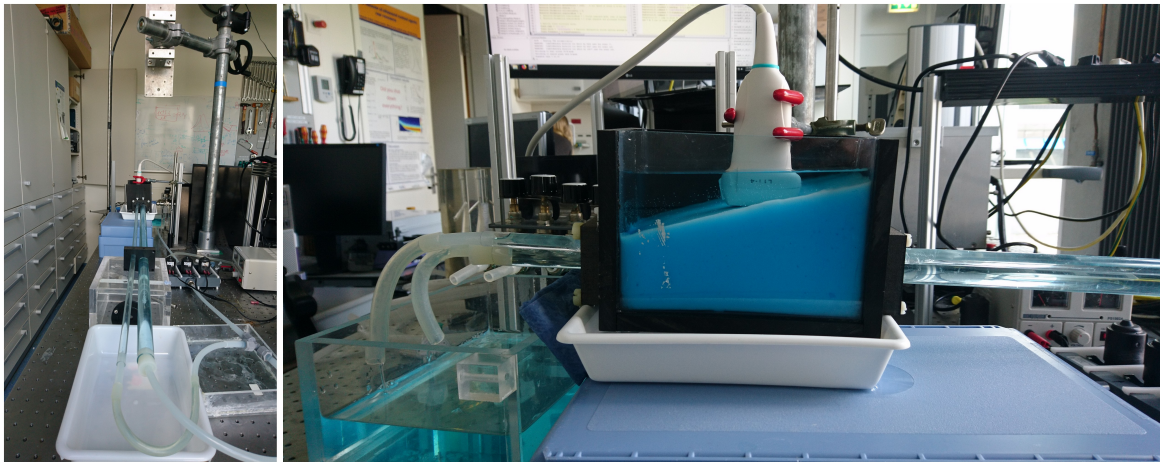


Figure 3.5: *In-vitro flow measurement set-up.*

Before gel preparation, two straight tubes ($\varnothing_{1,2} = 1$ cm and 2 cm) were placed within the mould to create a phantom of the femoral artery and abdominal aorta. After pouring the PVA mixture around the tubes in the mould, it underwent three freeze and thaw cycles (± 15 h & 9h, respectively). The mould was placed under an angle to create a tissue mimicking ultrasound model that simulates a slim and a more obese patient. The PVA phantom can be seen in figure 3.5.

The phantom was connected to a gearpump to generate continuous flow. To overcome any entrance effects, a rigid inlet section of 1.5m was placed in front of the phantom. The outlet of the phantom debouches into a reservoir where the UCA could be added before a UCA measurement.

Verasonics imaging sequences

A graphical user interface (GUI) of Verasonics was adapted so object parameters could be changed during run-time. Parameters like the transmitted voltage, time gain control and the dynamic range can be adjusted during run-time. Next to that, raw RF data and beamformed IQ data can be saved using the GUI.

Imaging sequences were tested and improved in multiple iterative cycles to achieve better visualisation. Plane wave (PW) US was applied for visualisation of the femoral artery. PI with PW US was applied for monitoring the bubbles. A linear L11-4v transducer was used ($f_0 = 4.03$ MHz) and the voltage was set to 10 Volts. All the measurements were performed with continuous flow. Prior to a UCA measurement, a reference measure was performed. Hereafter a dose of 0.5 millilitres Sonovue was injected for each UCA measurement in the phantom reservoir.

Measurement 1

A 1-angled PW and PI imaging sequence was tested on the femoral part of the phantom. The sampling frequency was set to 16 MHz. Theoretically, the Nyquist frequency of 8 MHz could be detected but in practice only frequencies up to 6 MHz were registered. The pulse repetition time was set to 100 μ s, while the frame rate was set to 10 Hz. In total 100 images were captured and analysed per measurement (10 sec).

Measurement 2

This measurement was performed on the abdominal aortic part of the phantom because of set-up limitations. At the time of the measurement, the L11-4v transducer was electrically approved by the technical support of Rijnstate hospital. To keep patient safety guaranteed, the probe should be kept within the hospital. Therefore the in vitro study was continued at Rijnstate hospital with limited materials. Although depth and diameter of the aortic tube differs from the femoral tube, imaging sequences could still be tested.

The imaging sequence was optimised by adding three angles (-0.3142, 0 and 0.3142 rad). 3-angled PW was applied for anatomy visualisation and a PI scheme with 3 non-inverted and 3 inverted angled PW were transmitted for bubble monitoring. One UCA measurement was performed with an acquisition sampling rate of 16 MHz and one UCA measurement was performed with a sampling rate of 32 MHz in order to detect the harmonic content. In order to suppress the tissue from the contrast, the non-linear signals from the microbubbles were amplified by applying a 20th order butterworth high-pass filter ($f_{\text{cut}} = 7$ MHz). To gain more insight in the results, the raw RF-data was also filtered by a 20th order butterworth low-pass filter ($f_{\text{cut}} = 6$ MHz). Filtering was applied before image reconstruction. The pulse repetition time was kept equal (100 μs) while the frame rate was increased to 100 Hz. In total, 200 images were captured and analysed per measurement (2 sec).

Data analysis

The original RF data from one element in one frame (measurement 2) was summed and displayed in one figure. First, the different acquisitions were separated. Next, the echoes from the 3-angled non-inverted pulses were shown in 1 figure and the echoes from the 3-angled inverted pulses were shown in 1 figure. The residual signal was calculated by summing all the six acquisitions.

A "contrast-to-background" ratio (CBR) was quantified so tissue (PVA) suppression efficacy could be assessed. CBR was calculated according to equation 3.1:⁷⁸

$$CBR = 20 \log_{10} \frac{\overline{RMS}_{tube}}{\overline{RMS}_{tissue}}, \quad (3.1)$$

where \overline{RMS} is the time-averaged root-mean-square intensity within the tube or PVA phantom (tissue). First, the frames from one measurement were averaged over time. Second, the Matlab function *roipoly* was used to select a region of interest which returns a mask for mask filtering. Thereafter, the mask was used to calculate the \overline{RMS} intensity of the region of interest. The CBR in dB is depicted above the corresponding frames of a UCA measurement (fig. 3.6 and 3.8).

After beamforming the RF data into IQ data, one frame was depicted in a greyscale image at a 35dB dynamic range (fig. 3.6 and 3.8). To gain insight in the effect of the chosen US settings and filtering, the power spectra of the RF data from the tube was calculated. A discrete Fourier transform was applied on the RF data at a depth from 31.5 mm until 44 mm (measurement 2). The power spectrum of one frame is calculated by averaging the spectra of the receive data from six transmitted pulses (3-angled PI) over 128 elements. Both the power spectral density of the unfiltered and filtered data are shown in figure 3.9. The power spectra of the unfiltered data can be compared to the power spectra of the corresponding reference measurements before UCA administration.

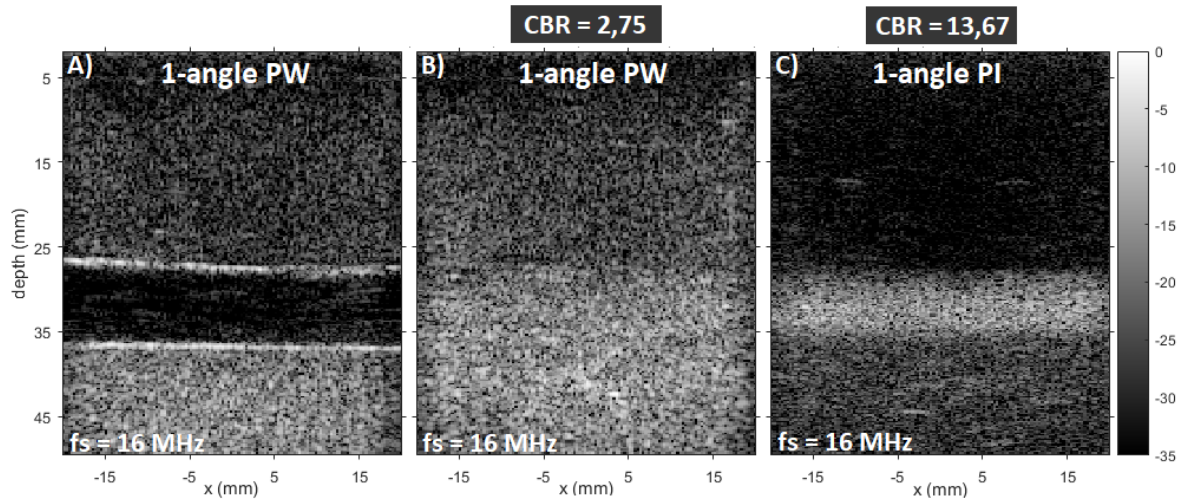


Figure 3.6: Measurement 1: PW-US frames of the femoral PVA phantom before (A) and after (B, C) UCA administration. The corresponding CBR (dB) is depicted above. Figure A and B were reconstructed from only the non-inverted PW and figure C was reconstructed from the summation of the PI pulses. Images displayed at 35dB dynamic range.

3.3.2 Results

Measurement 1

The in vitro results representing the visualisation of the femoral artery are depicted in figure 3.6. Figure 3.6.A was reconstructed from one non-inverted PW before UCA administration. The tube can be seen at a depth 27-37 mm. Because the RF data sampling rate was 16 MHz, harmonic components were not detected in the signal. Nevertheless, tissue scattering is considered to be (mainly) linear. Consequently a sampling rate of 16 MHz is sufficient to visualise tissue landmarks.

Figure 3.6.B and 3.6.C are reconstructed frames after UCA administration. The corresponding CBR is depicted above. The difference between these images stands out, although the acquisition was made in the same 10 seconds. The difference is that fig. 3.6.B was constructed from only the non-inverted PW and that 3.6.C was reconstructed from the summation of the non-inverted and the inverted PW. Because of the highly reflective microbubbles, backscatter was increased within the tube causing an increase in intensity at a depth of 27 mm in both figures. The straight tube is however not visible in the 1-angle PW figure (B). The image has become blurry at a depth of 27 mm and deeper. In figure C, the signals from the PVA phantom were suppressed using a PI imaging technique. The difference in intensity between the tube and the surrounding PVA tissue is confirmed by the calculated CBR. The intensity difference, caused by 1-angle PW, between the tube and the surrounding PVA phantom is small (CBR = 2,75 dB). The intensity difference in the 1-angle PI image is much larger, resulting in a CBR of 13,67 dB.

Measurement 2

The RF data of 1 frame by 1 element is shown in fig 3.7. The data was obtained after a dose of 0.5ml Sonovue. Fig. 3.7A displays the echoes from the non-inverted pulses that were transmitted with three angles (blue line:-0.3142 rad; red line: 0 rad; yellow line:0.3142 rad). Likewise, the echoes from the inverted pulses are shown in fig. 3.7B. The received signals in fig.3.7A and 3.7B seem identical. However, due to the opposite polarity of the transmitted waveforms, they are not. This is confirmed by the residual signal after summing all the six acquisitions. The amplitude of the residual became much smaller because the linear echoes from the non-inverted pulses (fig A) and the inverted pulses

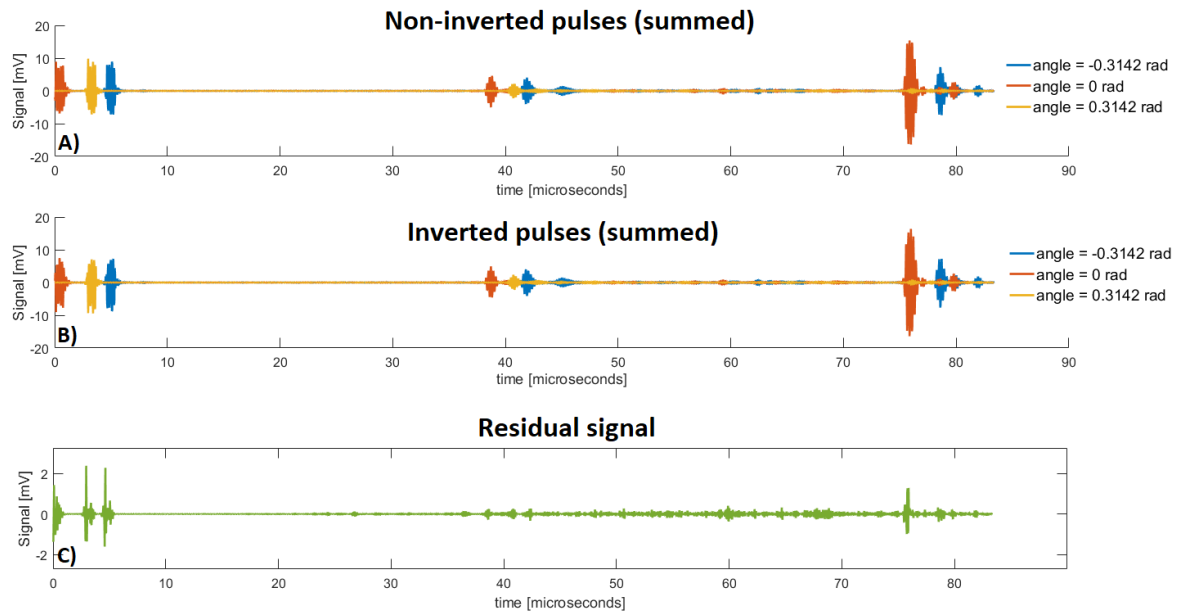


Figure 3.7: Measurement 2: The RF data of 1 frame by 1 element. The data illustrates the steps in the reconstruction of a PI image; the echos from the three non-inverted pulses (A) and the echos from the three inverted pulses (B) are summed to form the residual signal (C; green line). The blue, red and yellow indicate the steering angles of the US pulses (-0.3142 rad, 0 rad and 0.3142 rad respectively).

(fig B) cancel each-other out.

The images obtained during measurement 2 are depicted in figure 3.8 together with the corresponding CBR. The four images were obtained with a 3-angled PI acquisition scheme and a sample rate of 16 MHz (A) or 32 MHz (B, C and D). Some irregularities emerged in the phantom on top of the tube, due to degeneration of the PVA over time compared to measurement 1. The coloured line in the image refers to the corresponding power spectra within the tube, which can be found in figure 3.9. The spectra can be compared to the spectra of a reference measurement before UCA administration (dotted lines). The results are presented in the order of the images in figure 3.8 in a left-to-right and top-to-bottom order.

The tube in figure 3.8.A can clearly be distinguished from the surrounding PVA tissue. The highly scattering microbubbles are clearly visible. It is obvious that the spatial resolution is increased compared to figure 3.6.C which was obtained by only 1-angle PI. The difference in intensity between the tube and the surrounding tissue is confirmed by a CBR of 12,81. Nevertheless, the higher frequency components from the backscattering of the microbubbles could still not be detected ($f_s=16$ MHz) which is seen in figure 3.9 (yellow line). The magnitude peak around 4.4 MHz represents the fundamental frequency (f_0). The power spectral density within the tube before UCA was added to the flow (3-angle PI, $f_s=16$ MHz) is presented by the dotted yellow line. It can be seen that the yellow lines, solid and dotted, are alike. The figure shows that frequencies can be detected up to 6 MHz with a sample rate of 16 MHz.

The sample rate was therefore doubled to 32 MHz. The result is depicted in figure 3.8.B. The difference in intensity between the PVA phantom and the bubbles within the tube has become much smaller. The UCA are not clearly visible anymore which results in a rather low CBR of 1,96. The harmonic components in the signal are however noticeable in the power spectrum in figure 3.9 (red

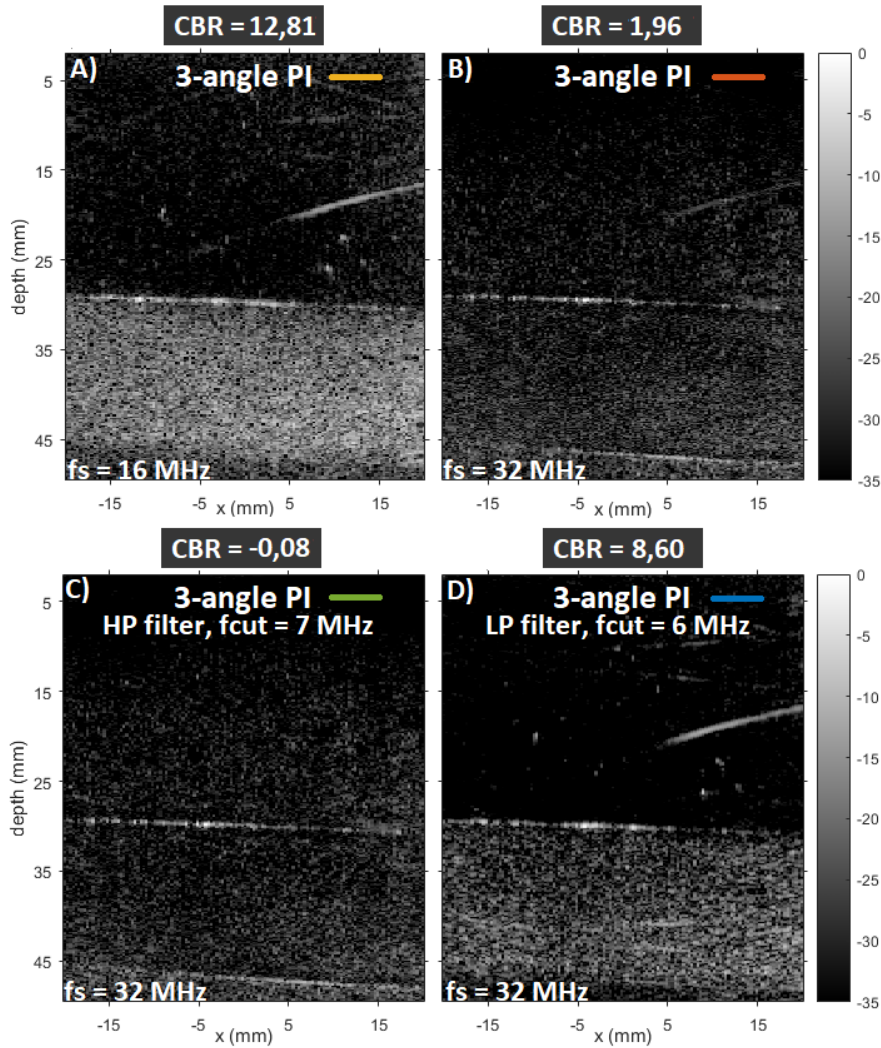


Figure 3.8: Measurement 2: PW-US frames of the aortic PVA phantom after UCA administration with corresponding CBR (dB). A 3-angled PI acquisition scheme was used with a f_s of 16 MHz (A) and a f_s of 32 MHz (B, C and D). The reconstructed high-pass and low-pass filtered RF data of figure B is shown in figure C and D respectively. Images displayed at 35dB dynamic range. The coloured lines refer to the spectral density in fig. 3.9.

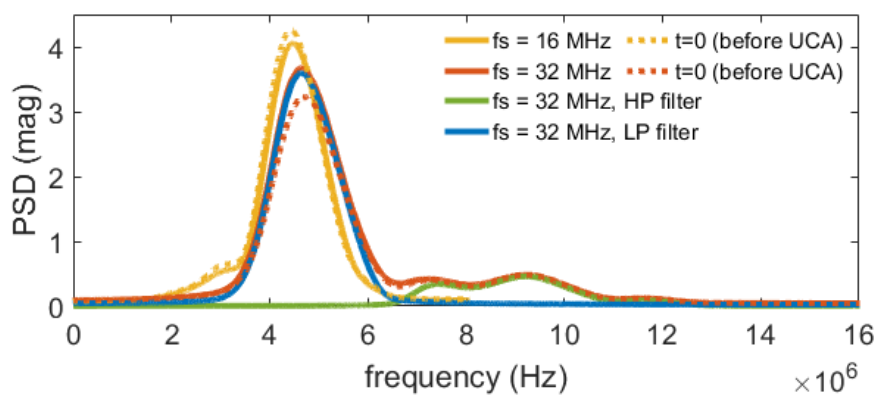


Figure 3.9: Spectral density of 3-angled PI data (within tube) of US measurements before (dotted) and after (solid) UCA administration. The colour of the line corresponds to the settings of the US images in fig. 3.8.

line). Besides the peak around the fundamental frequency, the spectrum consists of the second harmonic frequency around 9 MHz. Again, this power spectrum of a measurement after UCA administration can be compared to the power spectrum of a measurement before UCA administration (dotted red line). Also these power spectra are almost similar.

Figure 3.8.C shows the reconstructed high-pass filtered data obtained with with 3-angled PI plane waves and a sampling frequency of 32 MHz. It was expected that the filter amplifies the higher frequency components arisen from the microbubbles. Surprisingly, the intensity of the pixels within the tube are not increased compared to fig. 3.8.B resulting in even a lower CBR (-0.08). The tube can still be differentiated from the surrounding PVA material. The power spectral density of the high-pass filtered data is shown in figure 3.9 (green line). It can be seen that the second harmonic is still present while the fundamental frequency was filtered from the signal.

Figure 3.8.D shows the reconstructed low-pass filtered data (3-angled PI, $f_s=32$ MHz). The difference in intensity between the microbubbles in the tube and the surrounding tissue stands out immediately. Again, the microbubbles within the tube can be distinct easily resulting in a CBR of 8,60. The blue line in figure 3.9 illustrates the corresponding power spectral density. The fundamental frequency around 4.6 MHz is clearly visible while the harmonics were removed.

3.3.3 Discussion

Contrary to expectations, the high-pass filter did not improve the image quality in terms of CBR. Although the fundamental frequency was removed and the second harmonics was remained in the signal, it did not improve tissue suppression efficacy. All measurements in fig. 3.8 were made shortly after an amount of 0.5 ml Sonovue was added in the reservoir. It could be the case that there were fewer bubbles at the time of fig. 3.8B. However, it cannot explain the big difference in intensities between figures A and B. The PI images that relied on frequencies up to 6-8 MHz gave the best results (fig 3.8A and D). The calculated CBR confirmed these results. There are several possible explanations for this result.

Motion of tissue or UCA between the non-inverted and inverted pulse, that determines the cancellation of the signal, is not eliminated in the summed residual signal.^{58,82} The stationary PVA phantom did not cause any movement in contradiction to the microbubbles that were flowing through the phantom. Besides non-linearity, motion also contributed in the residual PI signal. The movement and the highly scattering properties of bubbles explain the high CBR, even when the harmonic components were not detected (fig. 3.8 A and D).

Non-linear propagation through tissue also explains the results partially. A constant velocity of the wave is required to maintain its shape as they propagate. A pulse, however, travels faster during the higher pressure phase compared to the lower pressure phase. This makes the pressure peaks propagate faster than the troughs evolving the sine wave more into a saw tooth wave.^{58,87} The wave becomes distorted affecting the wave's frequency structure. The wave will contain to a certain extent harmonic components. Although backscattering from tissue is approximately a linear process, the incident pulse can already be distorted through non-linear propagation and contain harmonics. Subsequently, the backscatter from tissue also contains harmonic frequencies.^{58,87} This in contradiction to the harmonic components created by the backscatter of microbubbles. These harmonic components originate from the moment of scattering and are not dependent on the distortion of the wave of the

incident pulse.⁵⁸ Both the harmonic signals arising from the bubbles as from non-linear propagation will be more present at higher acoustic power.^{58,87}

The power spectra in figure 3.9 suggest that the microbubbles produced very little harmonic frequencies. This because there were hardly differences in the spectra between the measurements with and without UCA. Following, it may be wondered if the microbubbles were insonicated properly. The oscillation of the microbubbles causes the non-linearity in the sound reflections, as discussed in section 2.3.^{60,61} It seems that the increase in CBR was mainly due to motion instead of non-linearity. The motion causes a reflection that mainly consists the fundamental frequency, which explain why the results that relied on frequencies up to 6-8 MHz gave the best results.

Further research should be undertaken to investigate why the UCA did not produce harmonic content. The acoustic power of insonation is defined by US pulse length and the mechanical index (MI).⁵⁸ Per transmit waveform only one ultrasound pulse was applied in the measurements. Therefore the duration of the PW was very short and could be an explanation why the bubbles were not oscillating and producing harmonics. Another explanation could be that the acoustic power was not sufficient. At low acoustic power, microbubbles exhibit signals with the same frequency as the excited US. Non-linear vibrations occur when the acoustic power of the US is increased.⁵⁸ This explanation is however questionable because non-linear scattering of microbubbles (usually) occurs even at very low pressure amplitudes ($\pm <0,03$ MPa).⁵⁸ A pressure measurement should be performed to calculate the acoustic output of the L11-4v transducer at 10 Volts ($f_0=4.03$ MHz). This measurement can estimate whether the MI was sufficient for microbubble insonification.

3.3.4 Conclusion

This in-vitro study was designed to determine optimal ultrasound settings for visualisation of the femoral artery and UCA monitoring in the in-vivo feasibility study. The tube and the UCA were clearly visualised. The results showed that image quality was improved by adding 3 angles of insonation. One unexpected finding was that the CBR was mainly defined by the movement of the bubbles, instead of the non-linear behaviour of the bubbles. Therefore the reconstructed images that relied only on the fundamental frequency, and thus the movement of the bubbles, gave the best results for UCA visualisation. Still, it was a phantom study and not all findings can directly be translated to the human body. In the feasibility study we still want to be able to measure harmonic content, so therefore the sample rate will be set to 32 MHz with a 3-angled PW and PI acquisition scheme for visualisation of the artery and UCA respectively.

Safety measurements

For this study, a Verasonics vantage 256 US device will be used. An L11-4v probe will be used to transmit and receive ultrasound waves in order to detect microbubbles. These research devices do not have the appropriate CE marking for clinical use and therefore safety measurements were performed to ensure patient safety. Different norms developed by the "International Electrotechnical Commission" (IEC) were used.

4.1 US output parameters

IEC 62359 specifies conditions regarding the field characterisations of medical diagnostic ultrasonic fields. According to this norm thermal and mechanical characteristics of the proposed probe and its settings must be determined.⁸⁸

4.1.1 Methods

Pressure measurements using a needle hydrophone were performed to test the acoustic output parameters of the probe.

Materials

- Watertank
- Verasonics vantage 256 US device
- Fibre optical hydrophone (FP124-05, Precision Acoustics)
- L11-4v probe
- Fixation arm
- BNC Oscilloscope
- Picoscope 5000 Oscilloscope

Set-up

A fibre-optic hydrophone is placed within a programmable fixation arm. A thin polymer film at the tip of the fibre sensor works on the principle of interferometric detection. Changes in thickness of the polymer film are induced acoustically.⁸⁹ Using the sensor calibration values, the measured voltage can be converted to an acoustic pressure.

The movement of the fixation arm is controlled in Matlab. The arm can move along the x- (lateral direction), y- (elevational direction), and z-axis (axial, or depth direction) in order to make a volume scan. The L11-4v probe is placed across the fixation arm at a (minimal) distance of 5 mm from the

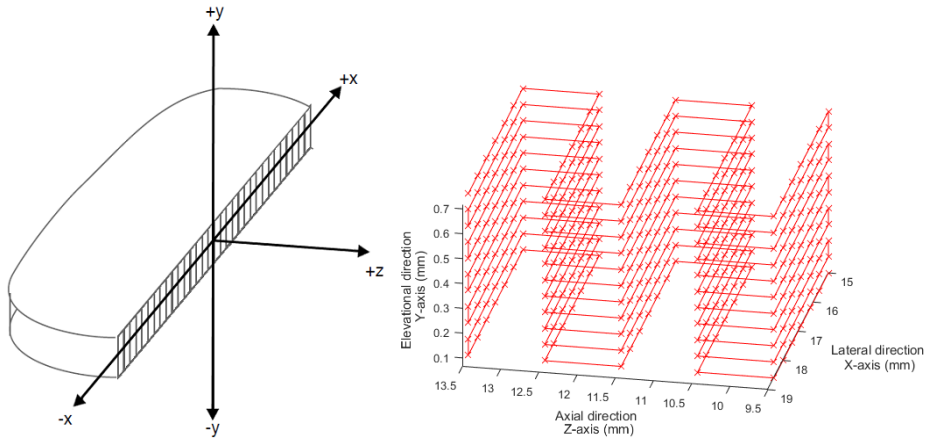


Figure 4.1: An example of the route of the fixation arm and hydrophone in order to scan a volume.

hydrophone. At each location, a single PW of 4 MHz is emitted from the L11-4v probe and recorded by the hydrophone. The maximum high voltage limit of the Verasonics US system is 50 volts and will be used as output level of the transducer. The measurements are performed in a filled water tank (figure 4.2).

It is important that all the signals are aligned. With a script in Matlab, the fixation arm is moved to the right position. The BNC oscilloscope triggers the Verasonics to emit a PW and the Picoscope to make a hydrophone measurement. After one measurement, the fixation arm moves to the next location until the desired volume is scanned and measured. The data of the Picoscope is saved in MATLAB along with the coordinates in order to connect the pressure measurements to the right locations.

Measurements

A raster scan was made to see which location in the US beam has the highest intensity. Hereafter new measurements around these locations were performed while spatial resolution was increased. The sampled volume is decreased in these measurements because only the locations of interest (highest intensity) will be used. An example route of the fixation arm of a scanned volume can be seen in figure 4.1.

Data analysis

The measured voltages can be converted to a pressure using the calibrated sensitivity of the fibre sensor. An attenuation coefficient of 0.3 is applied in order to correct for the attenuation of the echo signal in human tissue.

$$-0.3[dBcm^{-1}MHz^{-1}] \cdot depth[cm] \cdot f_{awf}[MHz] \quad (4.1)$$

According to equation 4.2, intensity can be calculated from the pressure signal:

$$I = \frac{p^2}{\rho \cdot c} \quad (4.2)$$

The Intensity (I) is calculated using the pressure (p), the density of water (ρ) and the speed of sound in water (c). Both the water density and the speed of sound in water are dependent on temperature. The water in the tank had an average temperature of 18 °C during the measurements.

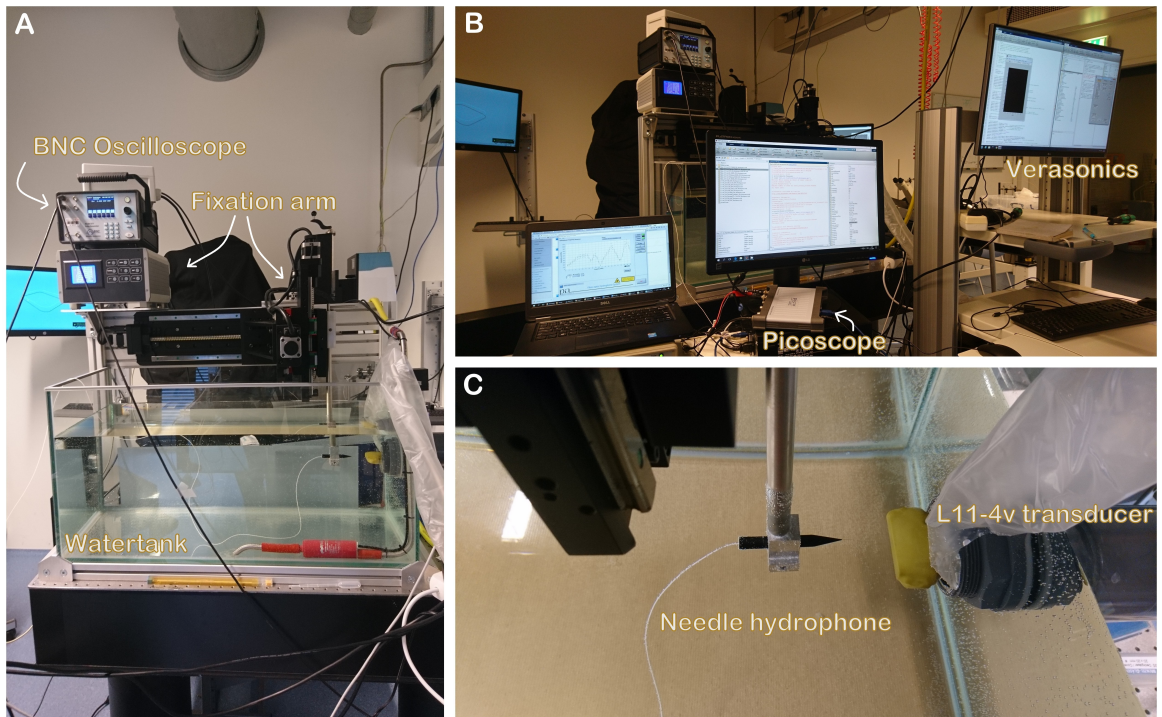


Figure 4.2: Measurement set-up. **A)** The transducer and the hydrophone are placed in a watertank. Above the watertank the BNC oscilloscope and the front panel and motor of the fixation arm can be seen. **B)** The Verasonics vantage 256 US device and the Picoscope 5000 Oscilloscope can be seen. **C)** Close up of the transducer, hydrophone and fixation arm.

The pulse intensity integral (PII) is given by the integral of the intensity signal over the duration of the pulse. According to IEC norm 62359 pulse duration is defined as 1.25 times the period between start- and end-time of the pulse. Start- and end-time was defined as the time point where the "relative intensity integral" was at 10% and 90% respectively.⁸⁸

The spatial-peak pulse-average Intensity (I_{sppa}) and the spatial-peak time-average Intensity (I_{spta}) can be calculated from the following equations:

$$I_{sppa} = \frac{PII}{pulseduration} \quad (4.3)$$

$$I_{spta} = PII \cdot PRF, \quad (4.4)$$

where PRF stands for pulse repetition frequency.⁸⁸ In the calculations, a PRF of 10 KHz is applied. The mechanical index, a measure of acoustic power, can be calculated by dividing the maximum rarefactional pressure P_r with the acoustic working frequency (f_{awf}) as stated in the following equation:

$$MI = \frac{P_r}{\sqrt{f_{awf}}} \quad (4.5)$$

The P_r is defined as the absolute value of the lowest measured pressure. The f_{awf} is defined as the mean of frequencies f_1 and f_2 at which the relative intensity is 3 dB below the peak magnitude.⁸⁸ The f_{awf} is determined by Fourier analysis. According to the United States Food and Drug Administration (FDA) norm for US systems and transducers, the acoustic output should not exceed the given

acoustic output exposure levels which can be seen in table 4.1. For peripheral vessels the MI, should not exceed 1.9.⁹⁰

4.1.2 Results

The smoothed echo pulses measured by the hydrophone needle can be seen in 4.3a. It can be seen that the ultrasound signal increases in voltage around 15 mm away from the transducer. When the distance increases between the transducer and the needle hydrophone, the amplitude of the ultrasound signal becomes smaller. This corresponds with the focus in depth (15-25 mm) of the L11-4v probe.⁸¹ Furthermore it can be seen that the asymmetry in the signals around y-axis increases with depth. The positive amplitude becomes larger compared to the negative amplitude when the distance from the probe increases. This is due to the non-linear propagation of the waveform which increases with distance travelled. This reshapes the waveform. The waveform measured close to the probe (5 mm) can be seen in figure 4.3b. The non-linear propagation is not visible yet. The frequency components present in the signal can be seen in the smoothed power spectral density in 4.3c. The fundamental frequency can be seen around 4.3 MHz. The first harmonics can be seen around 8.6 MHz and the second harmonics can be seen around 13 MHz. The first and second harmonics develop as depth increases. It can be seen that the harmonics are less present in the signal measured close to the probe (5 mm). The peaks in between are due to the tail of the lower frequency and the head of the higher harmonic frequency.

Plane scans

The acoustic output is shown by the PII. A top- and frontal scan can be seen in figure 4.4. The top view was made in the $y=0$ mm plane (fig.4.4a) and a clear focus can be seen at 15-20 mm depth. Again, this corresponds with the focus in depth of the L11-4v probe (15-25 mm). Because of this focus, the frontal view was made in the $z= 17.6$ mm plane (fig.4.4b). These plane scans indicate where the highest intensities can be found.

Volume scans

First a gross volume scan is made in the focus areas seen in figure 4.4. The results can be seen in figure 4.5. The highest intensities occur at the lateral sides of the beam profile. The red square indicates where the highest intensities occur and therefore indicates where the next near field scan is made. Following, a near field scan is made in the focus area at the lateral side of the beam profile. The results can be seen in figure 4.6a. Again, the highest intensity is indicated by a red square so spatial resolution can be increased. Finally, a near field volume scan is made in the focus area seen previously. The results can be seen in figure 4.6b. The red X indicates the highest measured intensity. This intensity is used to calculate the maximal acoustic output seen in table 4.1.

4.1.3 Conclusion

As seen in table 4.1, the acoustic output levels of the L11-4v transducer, using an emitting frequency of 4 MHz and a voltage of 50 Volts, are well within FDA guideline limits.⁹⁰ These values are defined for the use without injected UCA. An MI value of 0.7 is chosen as the threshold for cavitation and therefore the British Medical Ultrasound Society (BMUS) recommends to use a $MI < 0.7$ when an UCA is used.⁹¹ Therefore the voltage output level of the transmitters will be kept low (max 10V).

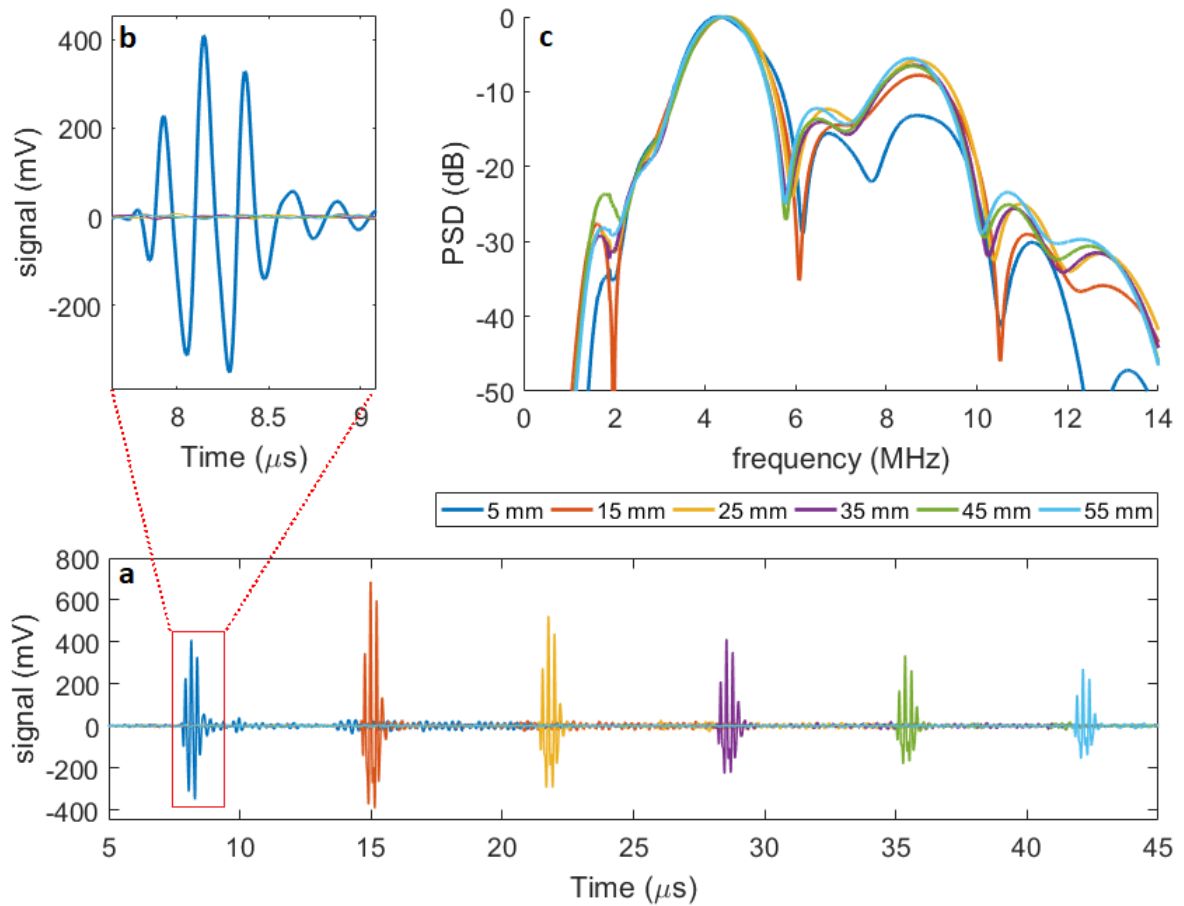


Figure 4.3: **a, b)** Ultrasound signals measured by the hydrophone needle at several distances from the echo transducer.
c) Power spectral density of the corresponding US signals.

	FDA safety criteria⁹⁰ (peripheral vessels)	L11-4v transducer (50V, 4 MHz)
ISPPA (W/cm^2)	190	75.2
ISPTA (mW/cm^2)	720	537.7
MI	1.9	0.97

Table 4.1: Maximum acoustic output.

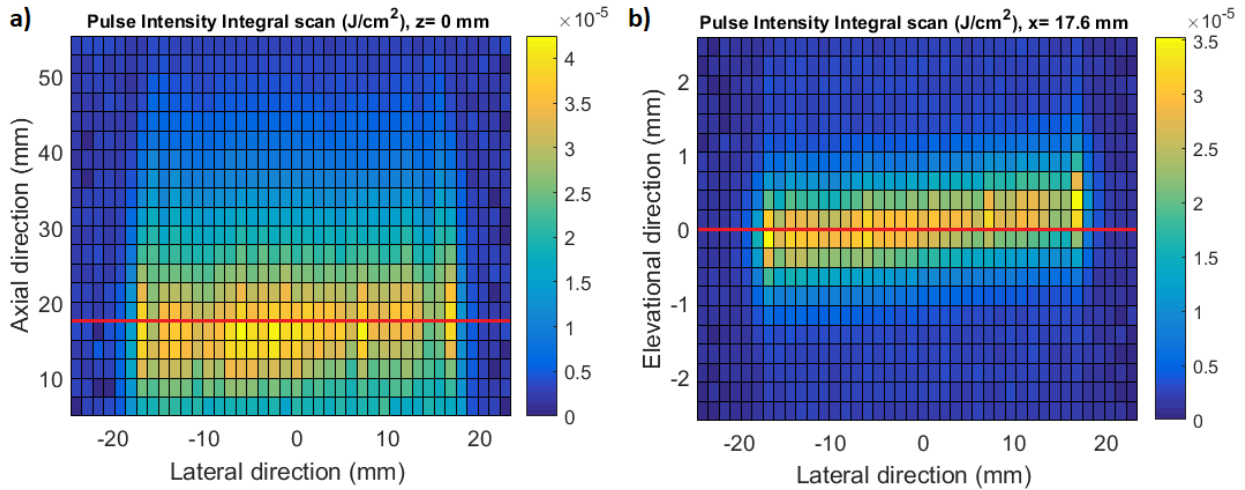


Figure 4.4: Top view (a) and frontal view (b) of beam profile. Red line indicates in which y- or z-plane the scan is made.

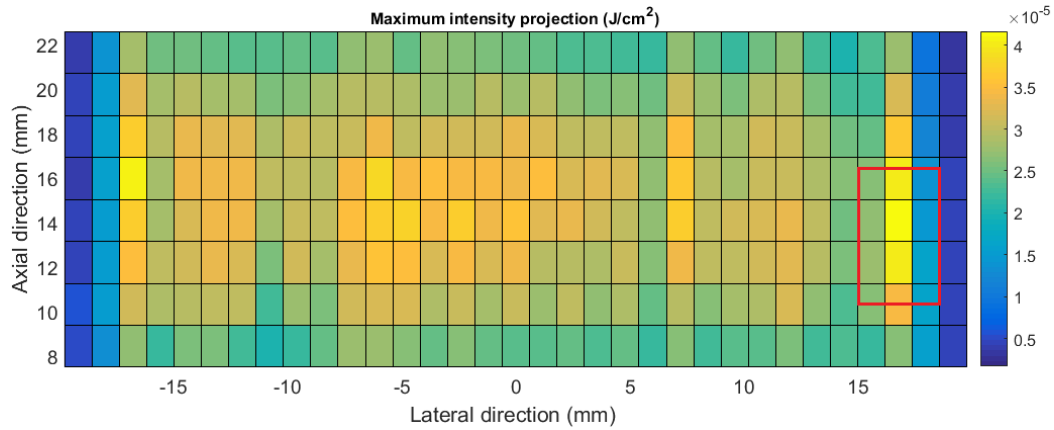


Figure 4.5: Maximum intensity projection (top view). The red square indicates in which volume a near field scan will be made.

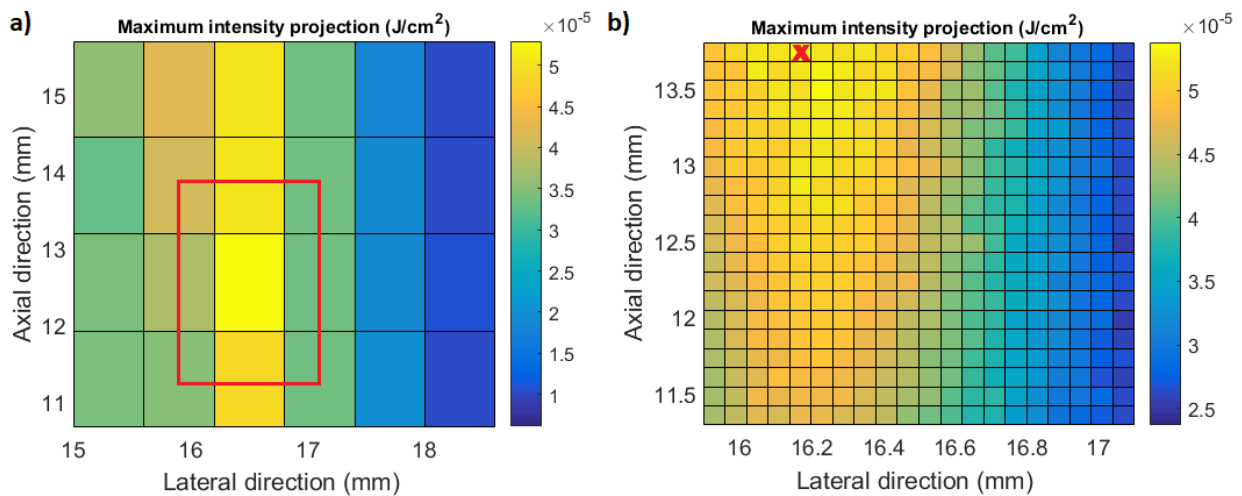


Figure 4.6: Maximum intensity projection (top view). **A)** a near field scan of the red square in fig. 4.5. The red square indicates the volume of the near field scan in fig. **B)**, where the X indicates the highest intensity.

4.2 Thermal measurements

Besides pressure measurements, temperature measurements were performed in order to ensure that the skin of the participant is not warmed up too much. The temperature of the skin can be increased by the absorption of US or by a heated probe surface. The temperature induced by the probe can be measured according IEC 60601-2-37, by a "still air" test using a thermal imager. The still air test should be performed with a stationary transducer in an ambient temperature of 23 ± 3 °C with minimal airflow around the probe. The duration of the measurement should be double the amount of time of the intended use, or up to 30 minutes. The maximum allowed temperature rise of the probe surface is 27 °C.⁹²

4.2.1 Methods

Temperature measurements using a thermal imager were performed to test the temperature rise of the transducer surface.

Materials

- L11-4v probe
- FLIR ONE 2nd Gen
- Tripod
- Verasonics vantage 256 US device
- Motorola Moto G4 Plus
- Transducer bracket

Set-up

The L11-4v transducer was placed within a portable bracket and connected to a Verasonics vantage 256 US device. The L11-4v probe was placed across the FLIR ONE thermal camera, which was mounted on a tripod system. The accuracy of the thermal camera is ± 3 °C or ± 5 % of the difference between ambient and scene temperature.⁹³ The recordings were visualised by the Motorola Moto G4 Plus that is connected to the camera. The set-up can be seen in figure 4.7.



Figure 4.7: Temperature measurements set-up. **A)** Measurements are visualized by a Motorola Moto G4 Plus. **B)** The stationary L11-4v transducer is placed in front of the FLIR ONE thermal camera.

Measurements

The measurements were performed in an ambient temperature of approximately 22.5 °C. According to IEC 60601-2-37, the initial temperature of the transducer should be the ambient temperature.⁹² The measurements were performed during HFR imaging and a live view setting. The live view setting will be used to visualise the femoral artery and UCA monitoring and the HFR settings will be applied for quantitative flow analysis. An emitting frequency of 4 MHz was applied during all measurements. For HFR imaging, the PRF was set to 10 KHz and the voltage to 20 and 50 Volts. The transducer was switched on for 10 seconds (double the scan time of 5 seconds) and measurements were repeated five times. For the live-view, the PRF was set to 100 Hz and the voltage to 50V, and switched on for 30 minutes.

4.2.2 Results

The temperature increase during one HFR measurement can be seen in figure 4.8. The start temperature is 23,7 °C and rises to an end temperature of 32.8 °C, which implies an temperature increase of 9.1 °C.

The greatest temperature rise was 9.7 °C when 50 Volts was applied and 1.2 °C when 20 Volts was applied. The temperature did not rise significantly during the 30 minutes of live view. The temperature keeps fluctuating between 23.4 and 23.8 °C. The results are schematically shown in figure 4.9.

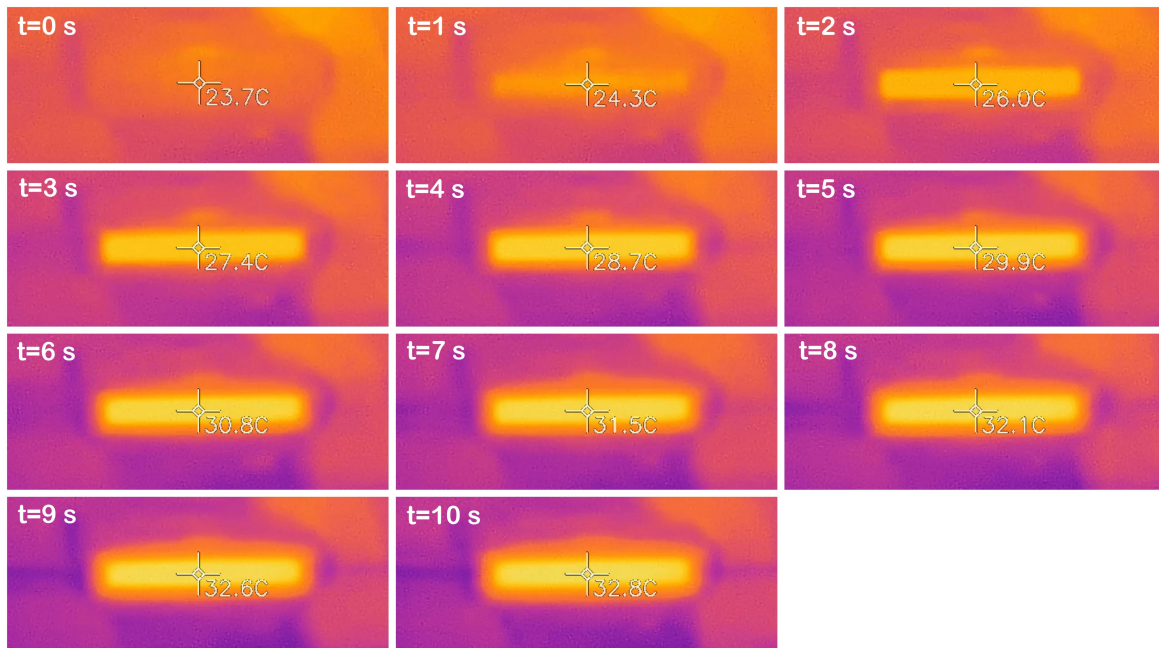


Figure 4.8: Thermal images of one HFR measurement where 50 Volts is applied. In 10 sec the temperature increases 9.1 °C.

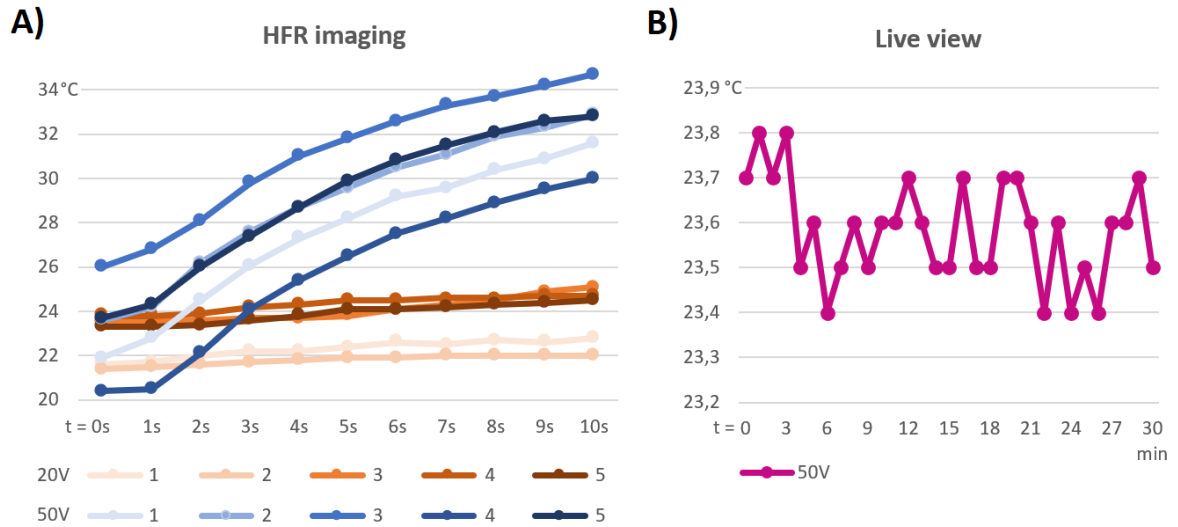


Figure 4.9: Thermal images of one HFR measurement where 50 Volts is applied. In 10 sec the temperature increases 9.1 °C.

4.2.3 Conclusion

The greatest increase in temperature was 9.7 C (50V) and 1.2 °C (20V) during HFR settings, while during the echoPIV measurements the voltage output level of the transmitters will even be kept lower (max 10V). There was no significant temperature rise seen during live view. The maximum allowed temperature rise of the probe surface is 27 °C according to IEC 60601-2-37.⁹² Therefore it can be concluded that the results are well within limits. The transducer can be used safely with the current settings in terms of the surface temperature rise.

Study protocol

This study protocol received approval the CCMO and the institutional review board of Rijnstate hospital (CCMO nr: 2018-4355). The study will be conducted according to the principles of the Declaration of Helsinki for Medical Research Involving Human Subjects Act and Good Clinical Practice (GCP) guidelines.

5.1 Introduction

The future research question is whether flow derived parameters could predict atherosclerotic disease progression, and thus could predict whether an individual patient or a specific stented lesion is more prone to subsequent development of (in-stent) restenosis, which is elaborated in the aim of this study in section 1.6. A previous study by our group, performed in healthy volunteers, showed the feasibility of echoPIV to quantify local flow patterns in the aortic bifurcation, through the use of HFR, contrast enhanced ultrasound (HFR-CEUS) measurements.¹² The objective of the current study is to determine the feasibility of femoral blood flow quantification near stented lesions using echoPIV. Results will be validated with CFD data that is obtained with patient-specific models. When feasibility is shown, a prospective cohort study will be planned in order to identify local flow patterns that can predict disease progression and stent patency in patients with PAD in the lower extremity.

5.2 Objectives

Primary Objective: To determine the feasibility of spatial and temporal quantification of blood flow near stents in the superficial femoral artery (SFA), using high framerate CEUS and particle image velocimetry (PIV).

Secondary Objective:

- Correlation of high framerate CEUS with computational fluid dynamics (CFD) data to validate the obtained results.
- Define predictors that could predict disease progression, stent patency and thus clinical outcome. When feasibility of echoPIV around and in stents in the SFA is shown, the predictors will be used to set up a prospective cohort study. In this study long term results can be linked to specific vessel geometries and flow characteristics visualised by echoPIV.

5.3 Study design

A feasibility study will be performed in patients with PAD who are treated with a stent in the SFA. Subjects will receive HFR-CEUS measurements. The obtained images will be used for PIV analysis, to obtain blood flow velocity data and to calculate flow derived parameters, such as WSS.

The data obtained with the CEUS measurements will be validated with 3D CFD data obtained through a femoral computational model. The patient-specific geometries of the model are extracted from a computed tomography angiography (CTA) scan after stent placement.

5.4 Study population

5.4.1 Population

20 PAD patients who recently received an endovascular treatment through a placement of a stent in the SFA will be included. The procedure may either be performed at an hybrid operating room or at an intervention room at the radiology department. A number of 20 is chosen to have enough variation in subject characteristics (heartrate, male vs. female, vessel geometries etc.). In this pilot study we plan to include 20 patients. Since the study has an explorative nature, a power calculation is not provided. Participants will be included from the outpatient clinic of the vascular centre in the Rijnstate Hospital, Arnhem. Before inclusion in the study, all procedures will be explained to the subjects and written information will be supplied. Informed consent will be obtained after a minimum of 48 hours, to give the subject time to reconsider what is asked.

Inclusion criteria	Exclusion criteria
<ul style="list-style-type: none"> • Scheduled endovascular treatment of a lesion in the SFA through placement of a bare metal or covered stent <p>or,</p> <ul style="list-style-type: none"> • A recently (<6 weeks) treated lesion in the SFA through placement of a bare metal or a covered stent 	<ul style="list-style-type: none"> • Hypersensitivity to the active substance(s) or any of the excipients in Sonovue • Right-to-left cardiac shunt • Severe pulmonary hypertension (pulmonary artery pressure > 90 mmHg) • Uncontrolled systemic hypertension • Severe pulmonary disease (e.g. COPD GOLD 3/4, ARDS) • Clinically unstable cardiac disease, prosthetic valves, congestive heart failure (class 3/4) • Hypercoagulable status, recent thrombosis • Loss of renal function (GFR < 31 ml/min) • End-stage liver disease • Sepsis • Hypersensitivity to iodinated contrast media • Pregnancy

Table 5.1: Inclusion and exclusion criteria.

5.4.2 Inclusion & exclusion criteria

In order to be eligible to participate in this study, a subject must meet one of the following inclusion criteria and none of the exclusion criteria in table 5.1.

5.5 Methods

5.5.1 Study parameters

Main study parameters:

Vector velocity fields derived from the echoPIV data will be used to calculate and visualise the velocity profile.

Secondary study parameters:

Vector velocity fields derived from the CFD data will be used to calculate and visualise the velocity profile and to validate the echoPIV results. Furthermore the wall shear stress (WSS) and the oscillatory shear index (OSI) will be calculated from both the echoPIV as the CFD data. Specific flow patterns, e.g. recirculation or blood stasis, will also be analysed.

5.5.2 Study procedures

CTA scan

CTA scans of the femoral artery will be performed at the start of the study in order to obtain the patient-specific geometries for the CFD model. The scan range is from the external iliac artery until the popliteal artery in the knee. A slice thickness of 1 mm has to be applied. The CTA scans will be performed after stent placement and before the first clinical follow-up moment in the outpatient clinic (6-8 weeks after treatment). Ideally, the CTA scan and the echoPIV measurement will be scheduled in one day. The CTA data will also be used for vessel wall delineation, to improve the calculation of WSS.

EchoPIV measurements

A Verasonics Vantage research US machine (Verasonics Inc, Kirkland, US-WA), with a L11-4v linear probe, will be used for the echoPIV measurements. This preclinical US machine is provided by the University of Twente and is not approved for general clinical use. All measures that were taken to ensure the safe use of the Verasonics US machine on the study subjects are discussed chapter 4.

Very low acoustic pressures are recommended because it has been shown that MIs of ≥ 0.06 in the region of interest can cause severe destruction of the UCA.⁷⁸ Moreover, higher MIs caused increased tissue intensity compared with UCA signal which is undesirable. MIs of 0.013 and 0.03 gave the best CBR values and did correspond to transmit voltages of 5V and 10V.⁷⁸ These voltages will also be applied in this feasibility study. Sonovue will be used as a contrast agent in all subjects.

Participants will receive echoPIV measurements in the vascular lab of the Rijnstate hospital. During the echoPIV measurements, an angled plane wave recording will be taken first to visualise the SFA. Only when the artery properly is visualised, a venous cannula will be placed. When the venous

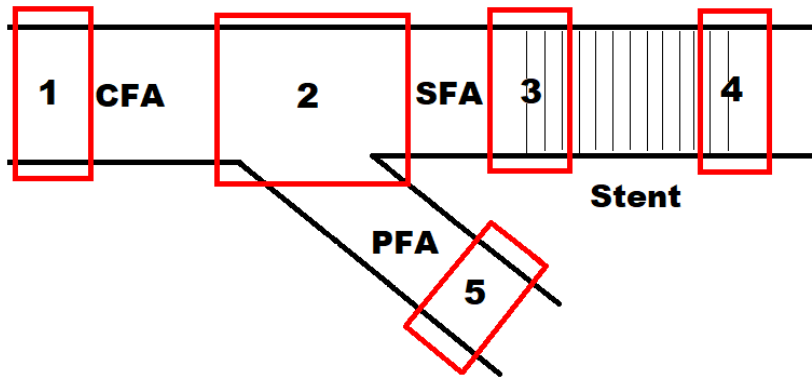


Figure 5.1: HFR-CEUS recording locations.

cannula is placed, a first 0.75 ml bolus of Sonovue will be administered, followed by a HFR-CEUS recording. This will be repeated five times so all regions of interest can be visualised. Totally, an amount of 3.75 ml Sonovue will be administered.

All locations are schematically visualised by the red squares in figure 5.1. The distance between different measurement locations is larger than schematically drawn. The velocity profile in the CFA (location 1) is required as input parameter for the CFD model. The femoral bifurcation is of interest because atherosclerosis preferentially develops at arterial branches and curvatures⁶ (location 2). The developed flow patterns can influence the inflow of the stent, which is thought to be of great importance regarding stent patency (location 3). The field of view of the transducer is 4 cm, therefore approximately 2 cm within and 2 cm outside of the stent will be visualised. The transition from stent to regular artery wall and how the stent affects blood flow will be visualised in location 4. The velocity profile at this location is also required as input parameter for the CFD model, like as the velocity profile in the PFA (location 5).

In total there will be 5 HFR-CEUS recordings. In each HFR-CEUS recording, images will be captured for 5 seconds (to ensure at least 3-4 full cardiac cycles are obtained) using an angled wave acquisition scheme and a pulse repetition frequency of 10 KHz.

Data processing

All HFR-CEUS data will be processed offline. Singular value decomposition based clutter suppression will be applied to the beam-formed data.⁷⁷ PIV analysis will be performed by means of block-wise cross-correlation using a modified version of PIVlab (V1.41).⁶⁷ Spatial and temporal smoothing will be applied on the obtained velocity vector fields.

5.5.3 Withdrawal of individual subjects

Subjects can leave the study at any time for any reason if they wish to do so without any consequences. The investigator can decide to withdraw a subject from the study for urgent medical reasons. Subjects will be replaced if they left the study before echoPIV measurements were performed. For all subjects who are prematurely withdrawn, the reason will be documented carefully.

In vivo echoPIV - preliminary results

6.1 Introduction

In this chapter, the in-vivo feasibility study is elaborated. The aim of the study was to determine the feasibility of femoral blood flow quantification near stented lesions in the superficial femoral artery using echoPIV. The preparations for this study can be read in the previous chapters. Considerations regarding the transducer and its settings can be found in chapter 3. Because a Verasonics US research device does not have the appropriate CE marking for clinical use, safety measurements were performed to guarantee patient safety. The US settings presented in the methods meet the safety criteria, which can be read in chapter 4. The feasibility study will be conducted according to the study protocol, elaborated in chapter 5. So far, one patient has been included in the study. First insights, and recommendations for further conducting the patient study will be discussed in the following sections.

6.2 Methods

This study conformed to the good clinical practice guidelines and was approved by the Central Committee on Research Involving Human Subjects and the institutional review board of Rijnstate hospital (CCMO nr: 2018-4355). All participants provided written informed consent for participation in the study.

6.2.1 Participant screening

The study design was a feasibility study performed in 20 patients with PAD. Patients were selected from the outpatient clinic of the vascular centre in the Rijnstate Hospital, located in Arnhem. A recent (<6 weeks ago) stent placement in the SFA was the only inclusion criteria. Participants were screened for hypersensitivity to iodinated contrast media and the UCA (Sonovue, Bracco Imaging s.p.a. Milan, Italy) that was used. Study participants met none of the exclusion criteria, listed in table 5.1 in chapter 5.



Figure 6.1: (comparable) EchoPIV setup in the vascular lab in Rijnstate hospital. The vascular sonographer is visualising the anatomy while a researcher is controlling the Verasonics US device.

6.2.2 Study procedures

CT angiography

The participant underwent a CTA to obtain the patient-specific geometries for the CFD model (future work). Next to that, the CTA will be used to gain insight into lesion characteristics. Participants were scanned from the external iliac artery until the popliteal artery with a slice thickness of 1 mm.

Contrast-enhanced US

EchoPIV measurements were performed in the vascular lab in the Rijnstate Hospital (comparable set-up for abdominal scanning shown in fig. 6.1). Data was recorded with the participant in supine position. A venous cannula was placed, for UCA administration, only after the SFA was visualised properly with the research US machine.

EchoPIV measurements were performed using a Verasonics Vantage 256 US research machine and a 128-element linear array transducer (Verasonics Inc, Kirkland, US-WA; L11-4v probe). A 3-angled PW sequence was generated at a PRF of 6 KHz (transmit freq = 4,03 MHz, single cycle pulse) for HFR measurements. A 3-angled PI scheme (20V) at 100 fps was used for real-time display of the arrival of the UCA. Saturation of the UCA must be avoided to make the bubbles distinguishable for proper PIV analysis, though the density of the bubbles should be sufficient to trace their motion.⁸⁴ The PI acquisition was also used to generate a standard B-mode real-time display, enabling the vascular sonographers to navigate to the region of interest in the femoral artery. A clinical US machine (iU22 xMATRIX, Philips, Eindhoven, the Netherlands) was used as reference. The Colour-Doppler modality provided useful hemodynamic information and eased distinguishing arterial and venous flow.

10 echoPIV measurements were performed at 5 locations, schematically visualised in figure 5.1 in chapter 5. At each location, series of HFR data sets were collected in two acquisitions of 2.5 seconds to ensure at least 3-4 full cardiac cycles. The transmit voltages were 5V and 10V, respectively. First, two segments of data were captured without contrast in the femoral bifurcation (location 2). After this measurement, five doses of 0.75 ml UCA were injected followed each by the capture of two segments of data at the five locations. HFR capture was initiated when the first UCA bolus had passed resulting in a UCA equilibrium in the vessel. 2 seconds of PI data for the real-time display was saved at the femoral bifurcation while visualising the UCA.

6.2.3 Data analysis

CT angiography

The analysis and interpretation of the CTA images was performed by a radiologist who reported about the status of the stent (open, stenosed or even occluded) and the other visualised arteries. In future work, the geometric data from the CTA will be implemented in a CFD model and will be used for vessel wall delineation, to improve WSS calculation.

Real-time CEUS data

Data analysis was performed to gain insight into the real-time US data at the femoral bifurcation. The power spectra of the RF data corresponding to the femoral artery, during diastole and systole, was calculated and could provide information about the harmonic behaviour of the UCA. The fundamental frequency was removed by applying a 16th order butterworth high-pass filter ($f_{\text{cut}} = 7$ MHz) to the RF data in order to amplify the harmonic frequencies. A 16th order low-pass filter ($f_{\text{cut}} = 6$ MHz) was applied to the data retaining only the fundamental frequency. High order filters were chosen to have a quick roll-off around the cut-off frequency. The RF data, both filtered (high-pass and low-pass) and unfiltered were reconstructed into images and displayed. To gain temporal insight in the low-pass filtered data, the averaged intensity differences over time of tissue and moving blood with UCA were compared.

HFR-CEUS data

SVD based clutter suppression was applied to the RF data as a method for tissue suppression and subsequently enhancing the UCA.⁷⁷ The results were compared with the original 3-angled PW data. Reconstructed images of the HFR-CEUS measurement, during diastole and systole were displayed. Tissue suppression efficacy was assessed by calculating a CBR according to the following equation;⁷⁸

$$CBR = 20 \log_{10} \frac{\overline{RMS}_{artery}}{\overline{RMS}_{tissue}}, \quad (6.1)$$

where the \overline{RMS} is defined as the (time-) averaged root-mean-square intensity within the specified tissue- or artery region. The regions are indicated by the yellow boxes in figure 6.6. Both the time-averaged CBR and the specific CBR for the shown frames were calculated. Furthermore, changes in pixel intensity over time in tissue, the CFA and the SFA were calculated and analysed for the 3-angled PW data and the SVD processed data. The pixel locations are indicated in fig. 6.6.

6.3 Results

1 participant was included (male, 78 years). All study measurements (echoPIV and CTA) were obtained successfully in one day, 3 weeks after stent placement.

6.3.1 Patient demographics

Patient characteristics include drug-controlled hypertension and hyperlipidemia, insulin-controlled diabetes, asymptomatic atrial fibrillation and the patient was not known with renal disease or pulmonary diseases. The patient did not smoke for the last 10 years.

The patient was diagnosed with TASC C femoropopliteal lesions; he had recurrent occlusions after an endovascular treatment in his left leg. Four years ago the subject received a short bare metal stent (2cm) in the proximal SFA and a bare metal stent (15cm) with a bending and helical design (LifeStent; Bard Peripheral Vascular Inc, Tempe, US-AZ) in the distal SFA. Both stents became occluded which caused complaints for the subject. The pre-procedural Duplex showed 2 short lesions (approximately 50%) in the proximal SFA, an occlusion in the distal part of the stent in the proximal SFA and an occlusion in the stent in the distal SFA. Therefore the subject recently received two heparin-bonded covered stents (VIABAHN Endoprosthesis; W. L. Gore and Associates, Flagstaff, US-AZ) that were placed from the proximal SFA into the popliteal artery, just above the femoral condyles (stent diameter: 6mm, total stent length: 25cm).

6.3.2 CT angiography

One coronal slice of the CTA is shown in figure 6.2. It shows a part of the upper left leg where the ilium and the pubic bone appears white. In between, the continuation of the CFA into the SFA and PFA is visible. The calcified plaques in the arteries can be clearly seen, especially in the CFA, the femoral bifurcation and the SFA. The stent was still functional and reported as open on the CTA scan.

6.3.3 Contrast-enhanced US

Real-time data

The vascular sonographers could visualise the femoral artery properly. Next to that, the arrival of the UCA could be monitored with the PI sequence. The analysed results of the real-time data can be found in figures 6.3, 6.4, and 6.5.

The spectral power density that corresponds to the femoral bifurcation at 24.5-26.5 mm depth (fig. 6.4), is depicted in figure 6.3. The spectrum contains both the frequency components during diastole (red line) and systole (purple line). It can be seen that the fundamental frequency is predominant, and no harmonic content can be recognised. Next to that, the diastolic- and systolic spectra are substantially equal.

Visual assessment indicated that the UCA could be visualised best with the low-pass filtered data. The non-filtered- and the high-pass data is therefore not shown. Two US images of the low-pass filtered data are shown on a 40dB dynamic range in figure 6.4. The image is shown along depth and the lateral direction (x). It can be

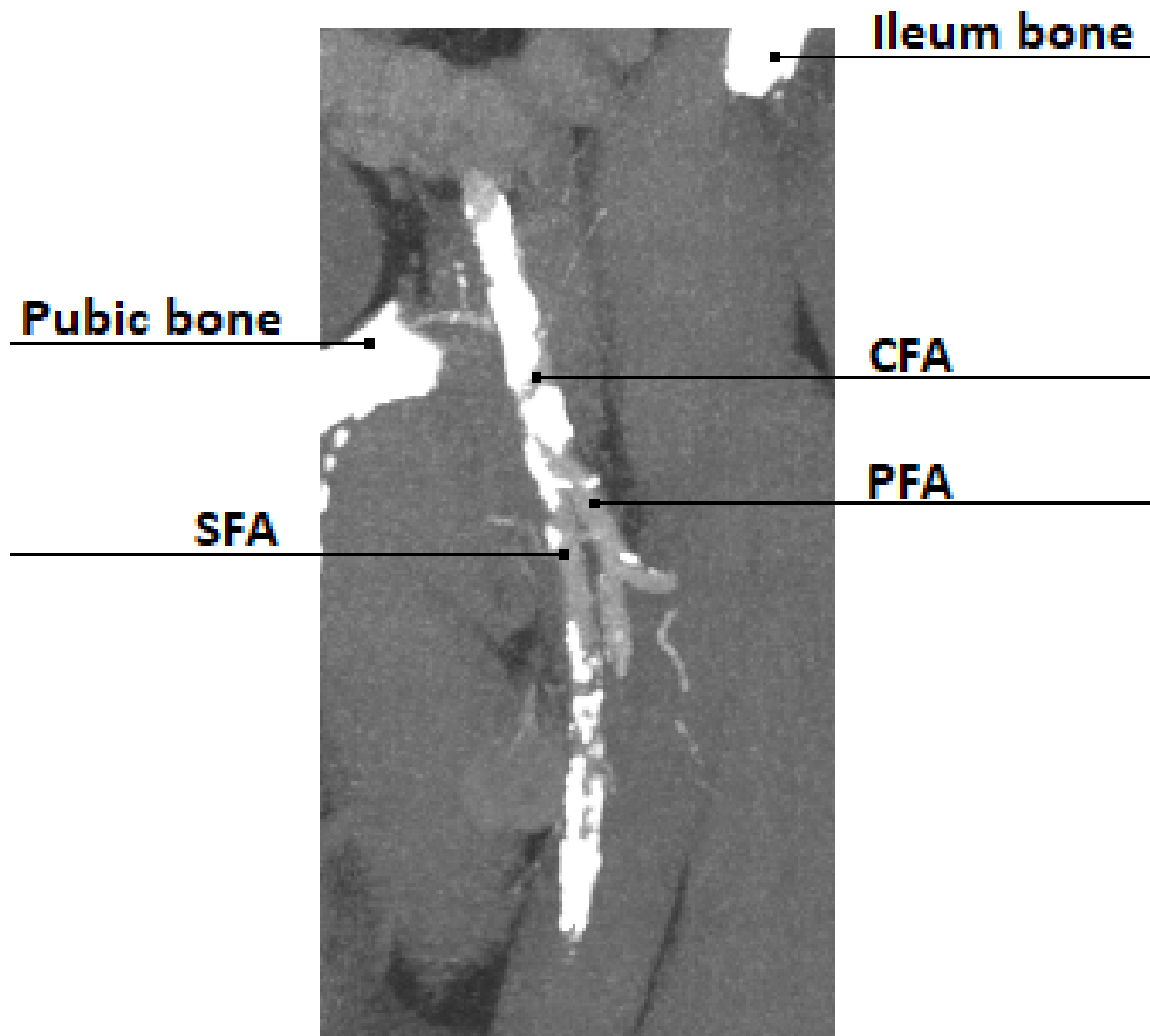


Figure 6.2: One coronal CTA slice of the femoral bifurcation in the left extremity.

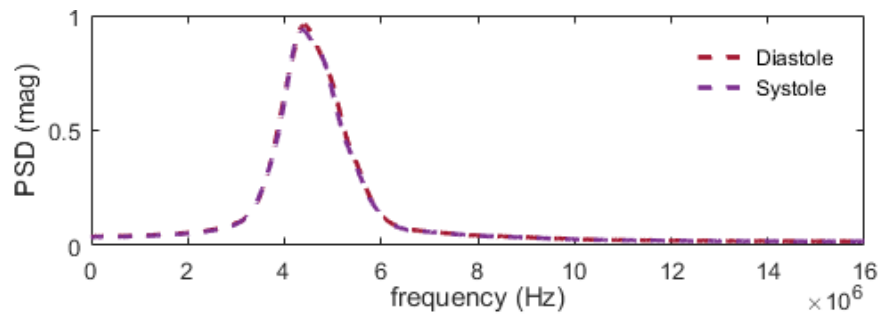


Figure 6.3: Real-time US; Power spectral density of original RF data during diastole (red line) and systole (purple line) corresponding with the femoral artery at a depth of 24.5 until 26.5 mm (shown in fig. 6.4). The fundamental frequency is predominant.

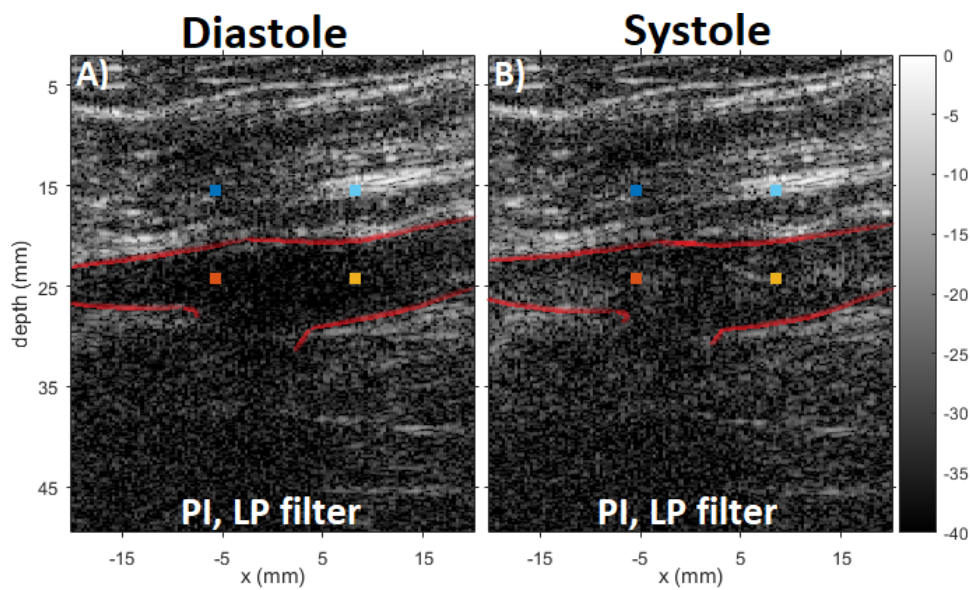


Figure 6.4: Real-time US; PI image of the femoral bifurcation during diastole (A, $t=0.45s$) and systole (B, $t=0.9s$). The red lines indicate the vessel anatomy. The CFA ($x < 0$ mm) bifurcates into the PFA and the SFA ($x > 0$ mm). The coloured squares refer to the locations of the intensity differences over time in fig. 6.5. Images displayed at 40dB dynamic range.

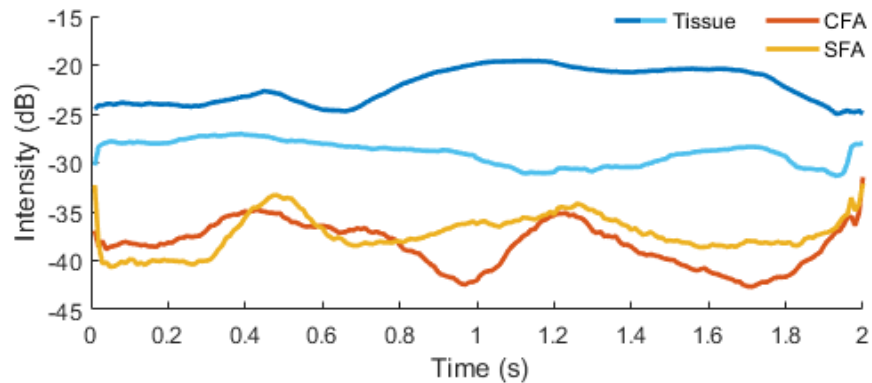


Figure 6.5: Real-time US; Averaged intensity changes over time within tissue (blue), the CFA (orange) and the SFA (yellow). The corresponding locations are shown in fig. 6.4

seen that the anatomical structures can be visualised properly, although the tissue does not seem to be suppressed much by the PI sequence. The CFA gives off the PFA, which is mostly out of plane, and the SFA. The red lines delineates the vessel wall. Very little microbubbles are present in the images during diastole (fig. 6.4A). During systole, a higher amount of UCA can be noticed (fig. 6.4B).

The differences in pixel intensity over time within tissue, the CFA and the SFA, in the regions indicated in fig. 6.4, are depicted in figure 6.5. It is apparent that the differences within the artery (orange/yellow) are much larger compared to the intensity differences within tissue (blue). The intensity peaks in yellow and orange ($t=0.5$, $t=1.25$ and $t=2.0$) corresponds to the systole of 3 cardiac cycles ($HR = \pm 80$ bpm). Next to that, higher intensities are identified in tissue.

HFR data

The reconstructed images and time-intensity plots of the CEUS-HFR data of the femoral bifurcation can be found in figures 6.6 and 6.7. SVD processing was performed manually on the 3-angled PW RF data. All frames were used when performing SVD (5040 frames). The modes with the lowest (<50) and highest (>800) singular values, respectively corresponding to tissue and noise, were removed.

PW and PW-SVD processed images during systole ($t=1.3s$) and diastole ($t=1.9s$) can be compared in figure 6.6. The images are displayed at a 40dB dynamic range. The red lines indicate the outlines of the femoral anatomy. It is difficult to recognise the femoral artery in the reconstructed images 6.6A and B from the 3-angled PW data. Only the SFA could be visualised and recognised properly in all images. It is more difficult to recognise the outlines of the CFA, visualised by the dashed red lines in figure 6.6C and D. The PFA branch cannot be recognised at all. Several tissue layers can be noticed on top of the femoral bifurcation. The yellow boxes in the figures indicate the locations that were used for CBR calculations as a method for tissue suppression quantification.

Figure 6.6A and B show the reconstructed images from the original 3-angled PW data during diastole (A) and systole (B). It is difficult to notice any differences in intensities between diastole and systole. Next to that, the tissue layers on top of the femoral bifurcation show the highest intensities. This is confirmed by the calculated CBR which is -18.01 dB and -18.07 dB, during diastole and systole respectively. The calculated time-averaged CBR of all frames (2.5s) is -17.93 dB.

The SVD processed images from the 3-angled PW data are shown in figure 6.6C and D. The femoral artery can be recognised more easily, due to the visibility of UCA in each heart cycle. Compared to the original PW images (6.6A and B), the tissue around the artery is suppressed through SVD processing. However, tissue layers in the top of the image can still be recognised. Next to that, the tissue below the femoral artery seems non-suppressed. A higher amount of UCA is visualised during systole (fig. 6.6D), compared to diastole (fig. 6.6C). These findings are confirmed by the calculated CBR. A CBR of -1.04 dB is found during diastole (fig. 6.6C). Signal strength in the specified region in the SFA is stronger compared to tissue signal in the specified yellow box during systole (CBR = 0.46 dB; fig. 6.6D). When all frames were taken into account (2.5s), a CBR of -1.82 dB was calculated. The coloured squares in fig. 6.6 indicate the locations in tissue, the CFA and the SFA, where the averaged intensity differences over time were calculated.

These graphs are shown in figure 6.7, that corresponds to the original 3-angled PW data (A) and the SVD filtered PW data (B). Prior to filtering, the tissue signal was stronger than the signals from

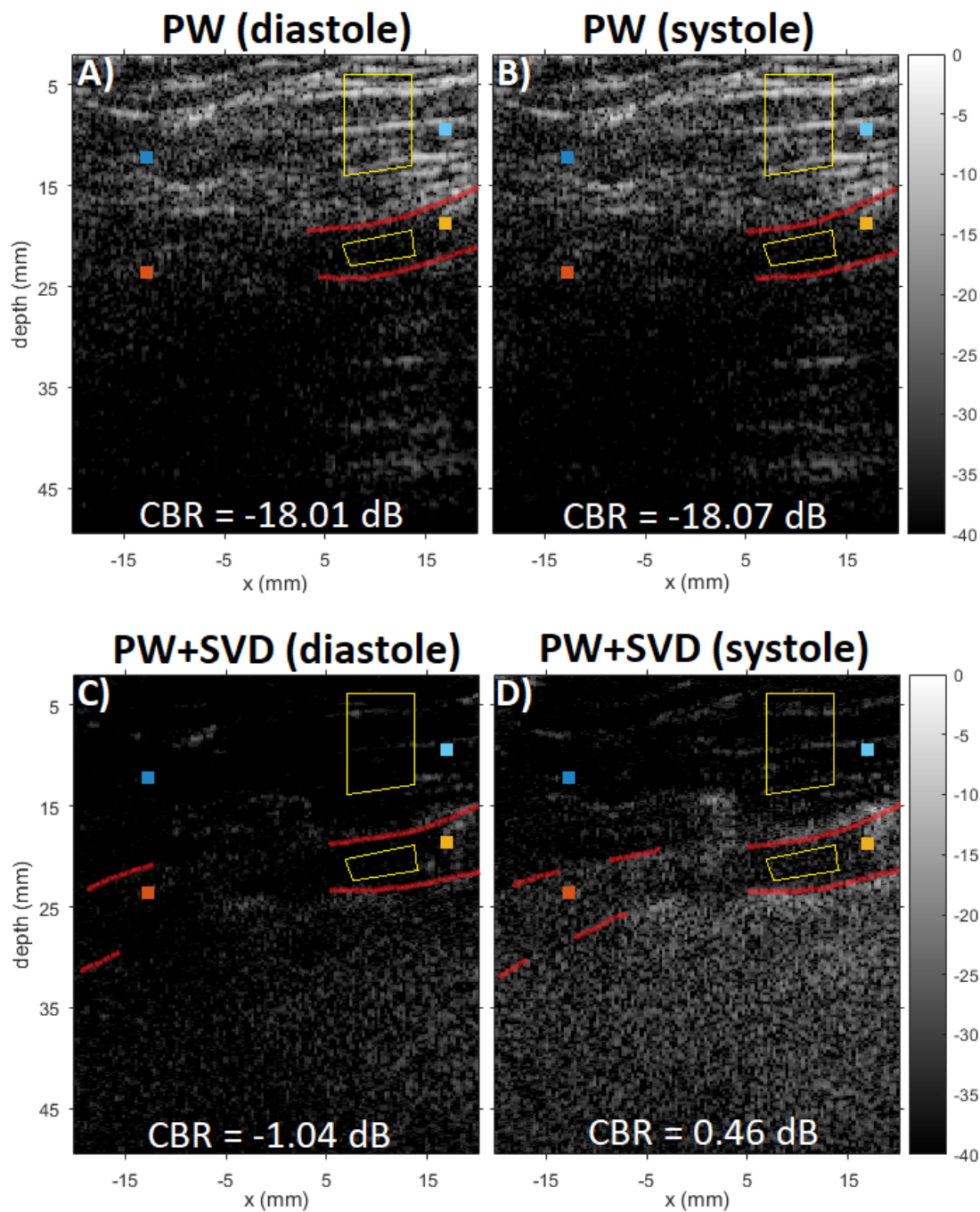


Figure 6.6: HFR US; 3-angled PW (A and B) and 3-angled PW-SVD processed images (C and D) during systole ($t=1.3s$) and diastole ($t=1.9s$). The red lines indicate the vessel anatomy. The yellow boxes indicate the regions for CBR calculation. The coloured squares indicate the locations of the intensities in fig. 6.7. Images displayed at 40dB dynamic range.

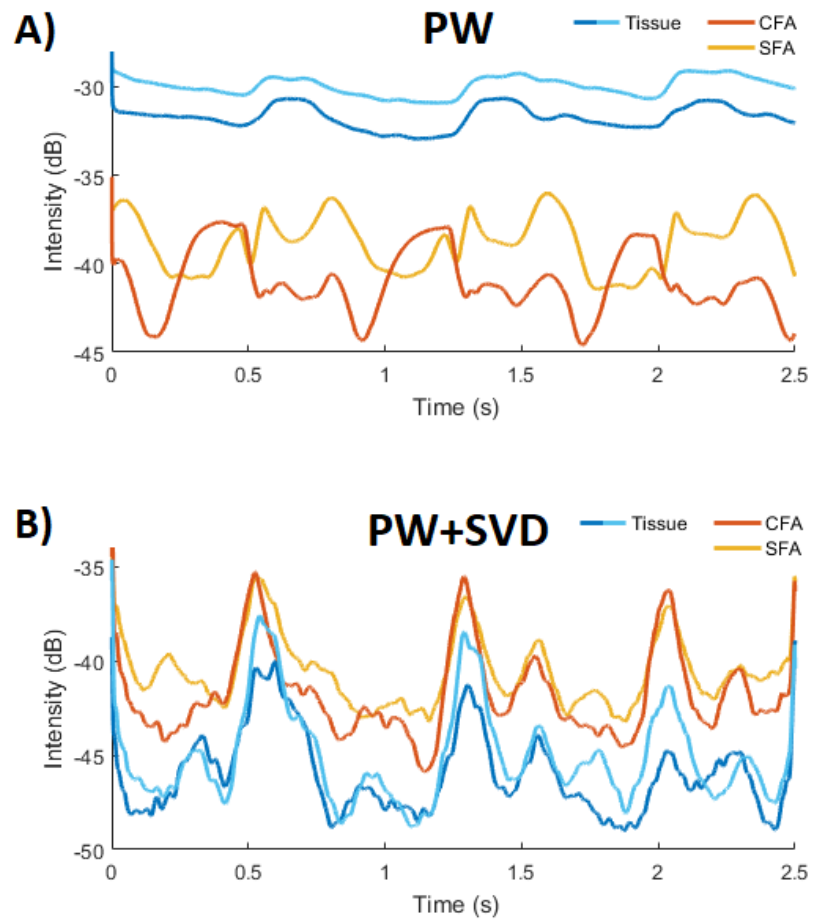


Figure 6.7: HFR US; Averaged pixel intensity changes over time within tissue (blue lines), the CFA (orange line) and the SFA (yellow line) of the 3-angled PW data (A) and the 3-angled PW SVD filtered data (B). The corresponding pixel locations are shown in fig. 6.6

the CFA and SFA as can be seen in fig. 6.7A. The difference in strength is approximately 7-8 dB. The tissue intensity was reduced as a result of SVD filtering, the intensities in the arteries became higher compared to tissue (fig. 6.7B). The intensities in the arteries became approximately 2-3 dB higher than in tissue.

In both figures, 3 full cardiac cycles can be appreciated from the intensity peaks during systole and intensity drops during diastole. The intensity peaks in figure 6.7B are very clear ($t=0.53s$, $t=1.29s$ and $t=2.05s$). Subsequently, a heart rate of 79 bpm is calculated. Besides the systolic peaks, more intensity peaks can be noticed in the figures. The orange intensity curve in fig 6.7B, corresponding to the CFA, shows a second peak after systole in the graph. Even three peaks can be recognised during the second cardiac cycle (1.1-1.9s) in the SFA (yellow line) in fig. 6.7B.

6.4 Discussion

The goal of the current study was to determine feasibility of echoPIV in the stented femoral artery. One patient with a recently placed stent in the SFA was included in the study and 6 HFR-CEUS measurements were successfully carried out. Both, the real-time CEUS (100 fps) and the HFR-CEUS measurement (2000 fps) in the femoral bifurcation was analysed and the results can be found in figures 6.3, 6.4, 6.5 and figures 6.6 and 6.7 respectively. The final goal of the project is to obtain blood flow velocity and -patterns and calculate flow derived parameters through PIV analysis of the HFR data. However, the currently available data does not have sufficient UCA signal to perform PIV analysis.

The poor visualisation of the UCA was surprising. Feasibility of echoPIV has been shown in the abdominal aorta in healthy volunteers.¹² The femoral artery is a more superficial artery compared to the abdominal aorta which should ease US imaging. Besides, US imaging in the lower extremity is not complicated by loss of US signal due to bowel gas. Therefore it was expected that image quality would increase and that PIV analysis could be performed with more ease. However, echoPIV has never been applied in patients with atherosclerotic disease. Next to that, only one patient was imaged so far and more measurements are required to draw conclusions. Several topics will be discussed and recommendations will be given for further conduction the feasibility study.

6.4.1 Real-time UCA monitoring

The PI sequence showed feasibility for monitoring the UCA. The low-pass filter outperformed the original data and the high-pass filtered data (not shown) for bubble visualisation. This confirmed the in-vitro results discussed in section 3.3. Because no harmonic content was clearly present in the spectrum (fig. 6.3) it is apparent that the high-pass filter, that eliminates the fundamental frequency, would not increase the CBR. The removal of the fundamental frequency would inherently decrease the signal-to-noise-ratio.⁹⁴ The low-pass filter that only retains the fundamental frequency, focuses on the signals arisen from the movement of the UCA. However, monitoring of contrast arrival could still be improved by utilising the non-linear properties of the UCA, for example by applying different US transmission schemes.

6.4.2 CEUS-HFR measurements

Both during diastolic- and systolic phases, SVD filtering performs better compared to the original 3-angled PW data in terms of CBR. The SVD filter effectively suppresses tissue because the pixel intensities of tissue were decreased (fig. 6.7) Still, results are by far not satisfying because PIV analysis could not be performed. Several improvements could be made in the SVD filtering, which was done manually. Both the highest and lowest rank-modes of the factorised SVD data were removed. A threshold selection algorithm could be implemented based on the spatio-temporal coherence reflected by the singular values.^{78,95} This could result in a better estimated separation between slow moving UCA and fast moving tissue. Fig. 6.7 shows that the intensities in tissue also change over time due to the cardiac cycle. This might be due to the pulsating artery that causes fast movement in tissue which is not removed by SVD filtering because it contains the same components as slow moving UCA that must be retained.

The size of the Casorati matrix also effects the separation between slow moving UCA and fast moving tissue.⁹⁴ It was shown that the CBR is improved by increasing the ensemble length during slow flow (diastole) and by decreasing the ensemble length during fast flow (systole).⁷⁸ The difference in spatial-temporal coherence between slow moving UCA and slow moving tissue during diastole is realised within time, and thus ensemble length. It was suggested that the pulsatile movement of the artery could be removed more easily with less frames and therefore increased the CBR.⁷⁸ This could however not explain the poor visualisation of the microbubbles during diastole, since an ensemble length of 5040 frames was applied. Furthermore, SVD filtering could be improved by performing it on the beamformed IQ data instead of the RF data.⁷⁸ Image quality might also improve by applying a background subtraction which could remove background interference, like tissue, to detect change over time in the artery.

Multiple cardiac cycles are visualised in figure 6.7 by the pixel intensity peaks of the UCA during systole. Normally a triphasic flow waveform is seen in the peripheral arteries, however due to atherosclerotic disease progression monophasic and biphasic flow patterns can also exist in the femoral artery.^{96,97} An increase in blood flow, regardless of which direction, causes an increase in pixel intensity in the artery. The second intensity peak in fig. 6.7 could therefore be due to reversed flow in the late systole arising from the high resistance outflow reflection, seen in biphasic and triphasic flow waveforms. The third intensity peak may be due to the second forward component during diastole, exhibited in triphasic flow patterns. Duplex US scanning of the subject showed only a minimal biphasic flow waveform in the CFA and a monophasic flow waveform in the SFA. Triphasic flow could however be noticed in the PFA, which suggests reversed flow from the PVA into the CFA in the subject during the HFR-measurements.

6.4.3 Acoustic power

Tuning the acoustic power is very important in velocity estimation through the use of microbubbles. In-vivo research has shown that already MIs of ≥ 0.06 in the region of interest can cause severe UCA destruction.⁷⁸ On the other hand, too low acoustic pressures may provoke insufficient UCA signal. No evidence was found for non-linear vibrations of the UCA because only the fundamental frequency was observed in the spectral density (fig 6.3), although the voltage was set to 20V in the PI real-time sequence. In-vitro results in section 3.3 where the transmit voltage was set to 10V, showed minimal harmonic content in the power spectra. The linear behaviour of the UCA could be due to a too low acoustic power that reaches the UCA. The MI is defined by the maximum rarefractional pressure (P_r)

and the acoustic working frequency (f_{awf}), as can be seen in equation 4.5 (chapter 4). Considering the resonant frequency of the UCA and the 11-4v transducer, an optimal frequency of 4 MHz was chosen and applied (section 3.2).

It is unfortunate that the applied MI is not known, only the maximal acoustic power at 50 volts was calculated during the safety measurements. The maximal MI was 0.97 at 13.7 mm depth (chapter 4). According to the L11-4v probe specifications, the elevation focus is at 20mm depth. The hydrophone measurement indicated an elevation focus of 11-19 mm depth (fig. 4.5). The femoral bifurcation of the subject is located just behind the elevation focus at 20-25 mm depth. Because the applied MIs are not known, it is recommended to perform new hydrophone measurements and calculate the MIs during a transmit voltage of 5V and 10V.

6.4.4 Patient echogeneity

The femoral arteries of the subject were severely calcified. The vascular sonographers indicated that it was difficult to visualise the femoral arteries and the stent, even with the clinical US machine that was used as a reference. The CTA slice in figure 6.2 shows calcified plaques in the CFA, femoral bifurcation and SFA. Weakening of the ultrasound beam by the plaques could also be a cause for the low acoustic power reaching the UCA. There are hardly any plaques recognised in the PFA, which in theory should result in more acoustic power reaching the UCA. However, both the 3-angled PW and the SVD filtered images gave poor image quality.

6.4.5 Pulse length

Besides the MI, pulse duration also effects the behaviour of the UCA and might be a cause for the non-harmonic content in the power spectra.^{58,98} Only a single cycle pulse PW with a frequency of 4.03 MHz was transmitted each acquisition and could be too short to insonificate the bubbles properly. At the cost of resolution, the effect of increasing the pulse length could be investigated by redoing the hydrophone measurements and calculate the MI. Moreover, in-vitro experiments can be performed to gain insight in the behaviour of the UCA.

6.4.6 US sequence evaluation

For the HFR data, it was shown that SVD processing outperforms the the original 3-angled PW data in terms of the CBR. However, bubble visualisation was still limited and therefore PIV analysis could not be performed. The lateral resolution can be increased by increasing the number of insonation angles.^{57,82} Too many acquisitions can, however, cause correlation loss between consecutive echoes due to the fast flowing UCA. Following, imaging artefacts arise within frames.⁸² Especially axial velocities affect image quality.⁸³ The clinical US machine measured increased peak systolic velocities of 170 cm/s in the CFA indicating that a high frame rate is desired. Next to that, an higher frame rate increases the spatial coherence between successive frames which improves SVD filtering.^{77,94}

It was surprising that the PI sequence during live-view could visualise the bubbles more clearly than the SVD processed HFR data. However, the voltage during live-view (20V) was twice as high than during the HFR measurement (10V) and could be the cause. Besides, the tissue did seem to be poorly suppressed. Though it would be interesting to learn whether the PI sequence could improve the HFR measurement. This will be at the cost of frame rate because both a non-inverted and inverted pulse have to be transmitted.⁷⁸ Following, image artefacts might arise. Hardware constraints

should also be taken into account. The PI pulses should have exact opposite polarity in order to cancel each other. Even minimal differences can cause unsatisfactory precision in the cancelling of stationary tissue.⁹⁴ More attention should be drawn to this process while further conducting the patient study.

Both AM and power modulated PI have been compared to SVD filtering in human vasculature.^{78,94} In both studies SVD filtering achieved a slightly better outcome in the visualisation of UCA while suppressing the tissue. The main advantage of SVD is that it does not require non-linear content within the echo to provide a successful separation between tissue and flowing blood with UCA.⁹⁴

6.5 Conclusion

HFR-CEUS measurements were performed successfully in one patient who was recently treated with a stent in the SFA. The vascular sonographer was able to visualise the femoral anatomy and monitor the UCA real-time with a Verasonics Vantage 256 US research machine and a linear L11-4v transducer. HFR data was processed by means of SVD filtering and provided an increased CBR compared with 3-angled PW. Still, the visualisation of the UCA was poor and therefore PIV analysis could not be performed. Several adjustments can be made to improve the HFR-CEUS measurement. Most importantly, the MI at imaging depth, with several transmitting voltages should be calculated so the acoustic power can be optimised. Also different transmit pulse schemes (e.g. pulse length, PI) should be investigated. Nevertheless, only one patient has participated in the study and more patient measurements are required before any conclusions can be drawn regarding the feasibility of echoPIV in the stented femoral artery.

Conclusions

EchoPIV could be a promising technique for the quantification of bloodflow around stents in the femoral artery, based on a previous study in the abdominal aorta.¹² This technique is clinically not yet available and has been introduced and implemented in Rijnstate hospital Arnhem during the past 12 months. A clinical feasibility study has been set up and the study protocol has been approved by the CCMO and the institutional review board of Rijnstate hospital. When feasibility can be shown, echoPIV can be used to gain insight into atherosclerotic disease progression and in-stent restenosis. One patient with lower extremity PAD has participated in the 'echoPIV in SFA' study and HFR-CEUS measurements could be performed successfully. UCA could be monitored real-time using a PI sequence. SVD processed images of the HFR PW data improved the CBR, PIV analysis could however not be performed due to poor visualisation of the UCA. This might be due to a decreased echogeneity in the patient because of the severe disease progression and the deposited calcified plaques in the femoral artery. UCA visualisation could be improved by utilising the non-linear behaviour of the UCA. The required adjustments should be investigated in-vitro. Only when feasibility of echoPIV around stents in the femoral artery is proven, it can be used as a method in a prospective cohort study identifying local flow patterns that can predict disease progression, in-stent restenosis and thus stent patency in patients with lower PAD.

Bibliography

- ¹ F Gerald R Fowkes, Diana Rudan, Igor Rudan, Victor Aboyans, Julie O Denenberg, Mary M McDermott, Paul E Norman, Uchechukwe KA Sampson, Linda J Williams, George A Mensah, et al. Comparison of global estimates of prevalence and risk factors for peripheral artery disease in 2000 and 2010: a systematic review and analysis. *The Lancet*, 382(9901):1329–1340, 2013.
- ² Victor Aboyans, Jean-Baptiste Ricco, Marie-Louise EL Bartelink, Martin Björck, Marianne Brodmann, Tina Cohnert, Jean-Philippe Collet, Martin Czerny, Marco De Carlo, Sebastian Debus, et al. 2017 esc guidelines on the diagnosis and treatment of peripheral arterial diseases, in collaboration with the european society for vascular surgery (esvs). *European heart journal*, 39(9):763–816, 2017.
- ³ Shahab Hajibandeh, Shahin Hajibandeh, Stavros A Antoniou, Francesco Torella, and George A Antoniou. Treatment strategies for in-stent restenosis in peripheral arterial disease: a systematic review. *Interactive cardiovascular and thoracic surgery*, 2018.
- ⁴ Ehrin J Armstrong, Haseeb Saeed, Bejan Alvandi, Satinder Singh, Gagan D Singh, Khung Keong Yeo, David Anderson, Gregory G Westin, David L Dawson, William C Pevec, et al. Nitinol self-expanding stents vs. balloon angioplasty for very long femoropopliteal lesions. *Journal of Endovascular Therapy*, 21(1):34–43, 2014.
- ⁵ Martin Schillinger, Schila Sabeti, Christian Loewe, Petra Dick, Jasmin Amighi, Wolfgang Mlekusch, Oliver Schlager, Manfred Cejna, Johannes Lammer, and Erich Minar. Balloon angioplasty versus implantation of nitinol stents in the superficial femoral artery. *New England Journal of Medicine*, 354(18):1879–1888, 2006.
- ⁶ Jeng-Jiann Chiu and Shu Chien. Effects of disturbed flow on vascular endothelium: pathophysiological basis and clinical perspectives. *Physiological reviews*, 91(1):327–387, 2011.
- ⁷ Daniel E Conway, Marcie R Williams, Suzanne G Eskin, and Larry V McIntire. Endothelial cell responses to atheroprone flow are driven by two separate flow components: low time-average shear stress and fluid flow reversal. *American Journal of Physiology-Heart and Circulatory Physiology*, 298(2):H367–H374, 2009.
- ⁸ Konstantinos C Koskinas, Yiannis S Chatzizisis, Antonios P Antoniadis, and George D Giannoglou. Role of endothelial shear stress in stent restenosis and thrombosis: pathophysiologic mechanisms and implications for clinical translation. *Journal of the American College of Cardiology*, 59(15):1337–1349, 2012.
- ⁹ Yiannis S Chatzizisis, Ahmet Umit Coskun, Michael Jonas, Elazer R Edelman, Charles L Feldman, and Peter H Stone. Role of endothelial shear stress in the natural history of coronary atherosclerosis and vascular remodeling: molecular, cellular, and vascular behavior. *Journal of the American College of Cardiology*, 49(25):2379–2393, 2007.

- ¹⁰ Fuxing Zhang, Craig Lanning, Luciano Mazzaro, Alex J Barker, Phillip E Gates, W David Strain, Jonathan Fulford, Oliver E Gosling, Angela C Shore, Nick G Bellenger, et al. In vitro and preliminary in vivo validation of echo particle image velocimetry in carotid vascular imaging. *Ultrasound in Medicine and Biology*, 37(3):450–464, 2011.
- ¹¹ Arati Gurung, Phillip E Gates, Luciano Mazzaro, Jonathan Fulford, Fuxing Zhang, Alex J Barker, Jean Hertzberg, Kunihiko Aizawa, William D Strain, Salim Elyas, et al. Echo particle image velocimetry for estimation of carotid artery wall shear stress: repeatability, reproducibility and comparison with phase-contrast magnetic resonance imaging. *Ultrasound in Medicine and Biology*, 43(8):1618–1627, 2017.
- ¹² Stefan Engelhard, Jason Voorneveld, Hendrik J Vos, Jos JM Westenberg, Frank JH Gijssen, Pavel Taimr, Michel Versluis, Nico de Jong, Johan G Bosch, Michel MPJ Reijnen, et al. High-frame-rate contrast-enhanced us particle image velocimetry in the abdominal aorta: first human results. *Radiology*, page 172979, 2018.
- ¹³ Kenneth Ouriel. Peripheral arterial disease. *The lancet*, 358(9289):1257–1264, 2001.
- ¹⁴ William R Hiatt. Medical treatment of peripheral arterial disease and claudication. *New England Journal of Medicine*, 344(21):1608–1621, 2001.
- ¹⁵ Heather L Gornik and Joshua A Beckman. Peripheral arterial disease. *Circulation*, 111(13):e169–e172, 2005.
- ¹⁶ David M Wootton and David N Ku. Fluid mechanics of vascular systems, diseases, and thrombosis. *Annual review of biomedical engineering*, 1(1):299–329, 1999.
- ¹⁷ Michael H Criqui and Victor Aboyans. Epidemiology of peripheral artery disease. *Circulation research*, 116(9):1509–1526, 2015.
- ¹⁸ Henri EJH Stoffers, Paula ELM Rinkens, Arnold DM Kester, Victor Kaiser, and J Andre Knottnerus. The prevalence of asymptomatic and unrecognized peripheral arterial occlusive disease. *International journal of epidemiology*, 25(2):282–290, 1996.
- ¹⁹ Wouter T Meijer, Arno W Hoes, Dominique Rutgers, Michiel L Bots, Albert Hofman, and Diederick E Grobbee. Peripheral arterial disease in the elderly: the rotterdam study. *Arteriosclerosis, thrombosis, and vascular biology*, 18(2):185–192, 1998.
- ²⁰ Peter Libby, Paul M Ridker, and Göran K Hansson. Progress and challenges in translating the biology of atherosclerosis. *Nature*, 473(7347):317, 2011.
- ²¹ James N Topper and Michael A Gimbrone Jr. Blood flow and vascular gene expression: fluid shear stress as a modulator of endothelial phenotype. *Molecular medicine today*, 5(1):40–46, 1999.
- ²² Michael A Gimbrone, Tobi Nagel, and James N Topper. Biomechanical activation: an emerging paradigm in endothelial adhesion biology. *The Journal of clinical investigation*, 99(8):1809–1813, 1997.
- ²³ Michael A Gimbrone, James N Topper, Tobi Nagel, Keith R Anderson, and Guillermo Garcia-Cardena. Endothelial dysfunction, hemodynamic forces, and atherogenesis. *Annals of the New York Academy of Sciences*, 902(1):230–240, 2000.
- ²⁴ Ira Tabas, Kevin Jon Williams, and Jan Borén. Subendothelial lipoprotein retention as the initiating process in atherosclerosis: update and therapeutic implications. *Circulation*, 116(16):1832–1844, 2007.

- ²⁵ Ira Tabas. Macrophage death and defective inflammation resolution in atherosclerosis. *Nature Reviews Immunology*, 10(1):36, 2010.
- ²⁶ Victor Aboyans, Michael H Criqui, Pierre Abraham, Matthew A Allison, Mark A Creager, Curt Diehm, F Gerry R Fowkes, William R Hiatt, Björn Jönsson, Philippe Lacroix, et al. Measurement and interpretation of the ankle-brachial index: a scientific statement from the american heart association. *Circulation*, 126(24):2890–2909, 2012.
- ²⁷ SB Coffi, D Th Ubbink, I Zwiers, AJM van Gorp, and DA Legemate. The value of the peak systolic velocity ratio in the assessment of the haemodynamic significance of subcritical iliac artery stenoses. *European Journal of Vascular and Endovascular Surgery*, 22(5):424–428, 2001.
- ²⁸ ML Bartelink, HEJH Stoffers, EJ Boutens, JD Hooi, V Kaiser, and LJ Boomsma. Nhg-standaard perifeer arterieel vaatlijden. In *NHG-Standaarden 2009*, pages 213–229. Springer, 2009.
- ²⁹ Ian Graham, Dan Atar, Knut Borch-Johnsen, Gudrun Boysen, Gunilla Burell, Renata Cifkova, Jean Dallongeville, Guy De Backer, Shah Ebrahim, Bjørn Gjelsvik, et al. Fourth joint task force of the european society of cardiology and other societies on cardiovascular disease prevention in clinical practice. *European Journal of Cardiovascular Prevention & Rehabilitation*, 14(2_suppl):E1–E40, 2007.
- ³⁰ Massimo F Piepoli, Arno W Hoes, Stefan Agewall, Christian Albus, Carlos Brotons, Alberico L Catapano, Marie-Therese Cooney, Ugo Corrà, Bernard Cosyns, Christi Deaton, et al. 2016 european guidelines on cardiovascular disease prevention in clinical practice: The sixth joint task force of the european society of cardiology and other societies on cardiovascular disease prevention in clinical practice. *Atherosclerosis*, 252:207–274, 2016.
- ³¹ Michael R TASC Steering Committee; Jaff, Christopher J White, William R Hiatt, Gerry R Fowkes, John Dormandy, Mahmood Razavi, Jim Reekers, and Lars Norgren. An update on methods for revascularization and expansion of the tasc lesion classification to include below-the-knee arteries: a supplement to the inter-society consensus for the management of peripheral arterial disease (tasc ii). *Vascular Medicine*, 20(5):465–478, 2015.
- ³² Lars Norgren, William R Hiatt, John A Dormandy, Mark R Nehler, Kenneth A Harris, and F Gerry R Fowkes. Inter-society consensus for the management of peripheral arterial disease (tasc ii). *Journal of vascular surgery*, 45(1):S5–S67, 2007.
- ³³ Scott M Surowiec, Mark G Davies, Shirley W Eberly, Jeffrey M Rhodes, Karl A Illig, Cynthia K Shortell, David E Lee, David L Waldman, and Richard M Green. Percutaneous angioplasty and stenting of the superficial femoral artery. *Journal of vascular surgery*, 41(2):269–278, 2005.
- ³⁴ John R Laird, Barry T Katzen, Dierk Scheinert, Johannes Lammer, Jeffrey Carpenter, Maurice Buchbinder, Rajesh Dave, Gary Ansel, Alexandra Lansky, Ecaterina Cristea, et al. Nitinol stent implantation vs. balloon angioplasty for lesions in the superficial femoral and proximal popliteal arteries of patients with claudication: three-year follow-up from the resilient randomized trial. *Journal of Endovascular Therapy*, 19(1):1–9, 2012.
- ³⁵ Martin Schillinger, Schila Sabeti, Petra Dick, Jasmin, Wolfgang Mlekusch, Oliver Schlager, Christian Loewe, Manfred Cejna, Johannes Lammer, and Erich Minar. Sustained benefit at 2 years of primary femoropopliteal stenting compared with balloon angioplasty with optional stenting.

- ³⁶ Patrick J Geraghty, Mark W Mewissen, Michael R Jaff, and Gary M Ansel. Three-year results of the vibrant trial of viabahn endoprosthesis versus bare nitinol stent implantation for complex superficial femoral artery occlusive disease. *Journal of vascular surgery*, 58(2):386–395, 2013.
- ³⁷ Mark W Mewissen. Self-expanding nitinol stents in the femoropopliteal segment: technique and mid-term results. *Techniques in Vascular & Interventional Radiology*, 7(1):2–5, 2004.
- ³⁸ G Tepe, J Laird, and P Schneider. Drug-coated balloon versus standard percutaneous transluminal angioplasty for the treatment of superficial femoral and/or popliteal peripheral artery disease: 12-month results from the in.pact sfa randomized trial. *Journal of Vascular Surgery*, 61(4):1098, 2015.
- ³⁹ John R Laird, Peter A Schneider, Gunnar Tepe, Marianne Brodmann, Thomas Zeller, Christopher Metzger, Prakash Krishnan, Dierk Scheinert, Antonio Micari, David J Cohen, et al. Durability of treatment effect using a drug-coated balloon for femoropopliteal lesions: 24-month results of in.pact sfa. *Journal of the American College of Cardiology*, 66(21):2329–2338, 2015.
- ⁴⁰ Michael D Dake, Gary M Ansel, Michael R Jaff, Takao Ohki, Richard R Saxon, H Bob Smouse, Lindsay S Machan, Scott A Snyder, Erin E O’leary, Anthony O Ragheb, et al. Durable clinical effectiveness with paclitaxel-eluting stents in the femoropopliteal artery: 5-year results of the zilvertx randomized trial. *Circulation*, pages CIRCULATIONAHA–115, 2016.
- ⁴¹ Johannes Lammer, Thomas Zeller, Klaus A Hausegger, Philipp J Schaefer, Manfred Gschwendtner, Stefan Mueller-Huelsbeck, Thomas Rand, Martin Funovics, Florian Wolf, Aljoscha Rastan, et al. Sustained benefit at 2 years for covered stents versus bare-metal stents in long sfa lesions: the viastar trial. *Cardiovascular and interventional radiology*, 38(1):25–32, 2015.
- ⁴² Richard R Saxon, Arun Chervu, Paul A Jones, Tanvir K Bajwa, Dennis R Gable, Peter A Soukas, Richard J Begg, John G Adams, Gary M Ansel, Darren B Schneider, et al. Heparin-bonded, expanded polytetrafluoroethylene-lined stent graft in the treatment of femoropopliteal artery disease: 1-year results of the viper (viabahn endoprosthesis with heparin bioactive surface in the treatment of superficial femoral artery obstructive disease) trial. *Journal of Vascular and Interventional Radiology*, 24(2):165–173, 2013.
- ⁴³ Eva Arvela, Maarit Venermo, Maria Söderström, Anders Albäck, and Mauri Lepäntalo. Outcome of infrainguinal single-segment great saphenous vein bypass for critical limb ischemia is superior to alternative autologous vein bypass, especially in patients with high operative risk. *Annals of vascular surgery*, 26(3):396–403, 2012.
- ⁴⁴ P Klinkert, PN Post, PJ Breslau, and JH Van Bockel. Saphenous vein versus ptfе for above-knee femoropopliteal bypass. a review of the literature. *European Journal of Vascular and Endovascular Surgery*, 27(4):357–362, 2004.
- ⁴⁵ Karen McQuade, Dennis Gable, Greg Pearl, Brian Theune, and Steve Black. Four-year randomized prospective comparison of percutaneous eptfe/nitinol self-expanding stent graft versus prosthetic femoral-popliteal bypass in the treatment of superficial femoral artery occlusive disease. *Journal of vascular surgery*, 52(3):584–591, 2010.
- ⁴⁶ Michel MPJ Reijnen, Laurens A van Walraven, Wilbert M Fritschy, Mare MA Lensvelt, Clark J Zeebregts, M Suzanna Lemson, Otmar RM Wikkeling, Luuk Smeets, and Suzanne Holewijn. 1-year results of a multicenter randomized controlled trial comparing heparin-bonded endoluminal to femoropopliteal bypass. *JACC: Cardiovascular Interventions*, 10(22):2320–2331, 2017.

- ⁴⁷ Andrea Holton, Edward Walsh, Andreas Anayiotos, Gerald Pohost, and Ramakrishna Venugopalan. Comparative mri compatibility of 316l stainless steel alloy and nickel–titanium alloy stents: Original article technical. *Journal of Cardiovascular Magnetic Resonance*, 4(4):423–430, 2002.
- ⁴⁸ Ragnhild Øvland. Coherent plane-wave compounding in medical ultrasound imaging: Quality investigation of 2d b-mode images of stationary and moving objects. Master's thesis, Norwegian University of Science and Technology, 2012.
- ⁴⁹ Sarah Dort, Stephan Muth, Abigail Swillens, Patrick Segers, Guy Cloutier, and Damien Garcia. *Vector flow mapping using plane wave ultrasound imaging*. PhD thesis, University of Montral, 2012.
- ⁵⁰ Maja Cikes, Ling Tong, George R Sutherland, and Jan Dhooge. Ultrafast cardiac ultrasound imaging: technical principles, applications, and clinical benefits. *JACC: Cardiovascular Imaging*, 7(8):812–823, 2014.
- ⁵¹ Jesper Udesen, Fredrik Gran, Kristoffer Lindskov Hansen, Jørgen Arendt Jensen, Carsten Thomsen, and Michael Bachmann Nielsen. High frame-rate blood vector velocity imaging using plane waves: Simulations and preliminary experiments. *IEEE transactions on ultrasonics, ferroelectrics, and frequency control*, 55(8):1729–1743, 2008.
- ⁵² Christian Poelma. Ultrasound imaging velocimetry: a review. *Experiments in Fluids*, 58(1):3, 2017.
- ⁵³ Jesper Udesen, Michael Bachmann Nielsen, Kristina Rue Nielsen, and Jorgen Arendt Jensen. Examples of in vivo blood vector velocity estimation. *Ultrasound in Medicine and Biology*, 33(4):541–548, 2007.
- ⁵⁴ Peter Møller Hansen, Jacob Bjerring Olesen, Michael Johannes Pihl, Theis Lange, Søren Heerwagen, Mads Møller Pedersen, Marianne Rix, Lars Lönn, Jørgen Arendt Jensen, and Michael Bachmann Nielsen. Volume flow in arteriovenous fistulas using vector velocity ultrasound. *Ultrasound in Medicine and Biology*, 40(11):2707–2714, 2014.
- ⁵⁵ Kristoffer Lindskov Hansen, Hasse Møller-Sørensen, Jesper Kjaergaard, Maiken Brit Jensen, Jens Teglgaard Lund, Mads Møller Pedersen, Jacob Bjerring Olesen, Jørgen Arendt Jensen, and Michael Bachmann Nielsen. Vector flow imaging compared with conventional doppler ultrasound and thermodilution for estimation of blood flow in the ascending aorta. *Ultrasonic imaging*, 39(1):3–18, 2017.
- ⁵⁶ Thomas L Szabo and Peter A Lewin. Ultrasound transducer selection in clinical imaging practice. *Journal of Ultrasound in Medicine*, 32(4):573–582, 2013.
- ⁵⁷ Jeremy Bercoff. Ultrafast ultrasound imaging. In *Ultrasound imaging-Medical applications*. InTech, 2011.
- ⁵⁸ Emilio Quaia. *Contrast media in ultrasonography: basic principles and clinical applications*. Springer Science & Business Media, 2005.
- ⁵⁹ Michalakis Averkiou, Jeff Powers, Dan Skyba, Matthew Bruce, and Seth Jensen. Ultrasound contrast imaging research. *Ultrasound quarterly*, 19(1):27–37, 2003.
- ⁶⁰ Flemming Forsberg, Barry B Goldberg, Ji-Bin Liu, Daniel A Merton, and Nandkumar M Rawool. On the feasibility of real-time, in vivo harmonic imaging with proteinaceous microspheres. *Journal of ultrasound in medicine*, 15(12):853–860, 1996.

- ⁶¹ PM Shankar, P Dala Krishna, and VL Newhouse. Advantages of subharmonic over second harmonic backscatter for contrast-to-tissue echo enhancement. *Ultrasound in Medicine and Biology*, 24(3):395–399, 1998.
- ⁶² Andrew W Appis, Melissa J Tracy, and Steven B Feinstein. Update on the safety and efficacy of commercial ultrasound contrast agents in cardiac applications. *Echo research and practice*, 2(2):R55–R62, 2015.
- ⁶³ Jean-Michel Correas, Lori Bridal, Amélie Lesavre, Arnaud Méjean, Michel Claudon, and Olivier Hélénon. Ultrasound contrast agents: properties, principles of action, tolerance, and artifacts. *European radiology*, 11(8):1316–1328, 2001.
- ⁶⁴ Douglas L Miller, Michalakakis A Averkiou, Andrew A Brayman, E Carr Everbach, Christy K Holland, James H Wible, and Junru Wu. Bioeffects considerations for diagnostic ultrasound contrast agents. *Journal of Ultrasound in Medicine*, 27(4):611–632, 2008.
- ⁶⁵ Jean-Marie Gorce, Marcel Arditi, and Michel Schneider. Influence of bubble size distribution on the echogenicity of ultrasound contrast agents: A study of sonovue. *Investigative radiology*, 35(11):661–671, 2000.
- ⁶⁶ Bracco International B.V. Sonovue: summary of product characteristics, April 2006.
- ⁶⁷ William Thielicke and Eize Stamhuis. Pivlab—towards user-friendly, affordable and accurate digital particle image velocimetry in matlab. *Journal of Open Research Software*, 2(1), 2014.
- ⁶⁸ KD Hinsch. *Particle image velocimetry*.
- ⁶⁹ Ajay K Prasad. Particle image velocimetry. *Current Science*, 79(1):51–60, 2000.
- ⁷⁰ Lingli Liu, Hairong Zheng, Logan Williams, Fuxing Zhang, Rui Wang, Jean Hertzberg, and Robin Shandas. Development of a custom-designed echo particle image velocimetry system for multi-component hemodynamic measurements: system characterization and initial experimental results. *Physics in Medicine & Biology*, 53(5):1397, 2008.
- ⁷¹ Hyoung-Bum Kim, Jean Hertzberg, Craig Lanning, and Robin Shandas. Noninvasive measurement of steady and pulsating velocity profiles and shear rates in arteries using echo piv: in vitro validation studies. *Annals of biomedical engineering*, 32(8):1067–1076, 2004.
- ⁷² Chee Hau Leow, Eleni Bazigou, Robert J Eckersley, CH Alfred, Peter D Weinberg, and Meng-Xing Tang. Flow velocity mapping using contrast enhanced high-frame-rate plane wave ultrasound and image tracking: Methods and initial in vitro and in vivo evaluation. *Ultrasound in Medicine and Biology*, 41(11):2913–2925, 2015.
- ⁷³ Réka Faludi, Mariola Szulik, Jan D’hooge, Paul Herijgers, Frank Rademakers, Gianni Pedrizzetti, and Jens-Uwe Voigt. Left ventricular flow patterns in healthy subjects and patients with prosthetic mitral valves: an in vivo study using echocardiographic particle image velocimetry. *The Journal of thoracic and cardiovascular surgery*, 139(6):1501–1510, 2010.
- ⁷⁴ Nico de Jong, Peter JA Frinking, Ayache Bouakaz, and Folkert J Ten Cate. Detection procedures of ultrasound contrast agents. *Ultrasonics*, 38(1-8):87–92, 2000.
- ⁷⁵ Antonio Stanziola, Matthieu Toulemonde, Yesna O Yildiz, Robert J Eckersley, and Meng-Xing Tang. Ultrasound imaging with microbubbles [life sciences]. *IEEE Signal Processing Magazine*, 33(2):111–117, 2016.

- ⁷⁶ Che-Chou Shen, Yi-Hong Chou, and Pai-Chi Li. Pulse inversion techniques in ultrasonic nonlinear imaging. *Journal of Medical Ultrasound*, 13(1):3–17, 2005.
- ⁷⁷ Charlie Demené, Thomas Deffieux, Mathieu Pernot, Bruno-Félix Osmanski, Valérie Biran, Jean-Luc Gennisson, Lim-Anna Sieu, Antoine Bergel, Stéphanie Franqui, Jean-Michel Correas, et al. Spatiotemporal clutter filtering of ultrafast ultrasound data highly increases doppler and ultrasound sensitivity. *IEEE transactions on medical imaging*, 34(11):2271–2285, 2015.
- ⁷⁸ J Voorneveld, S Engelhard, HJ Vos, MMPJ Reijnen, F Gijsen, M Versluis, E Groot Jebbink, N de Jong, and JG Bosch. High frame rate contrast-enhanced ultrasound for velocimetry in the human abdominal aorta. *IEEE transactions on ultrasonics, ferroelectrics, and frequency control*, 2018.
- ⁷⁹ Gene H Golub and Christian Reinsch. Singular value decomposition and least squares solutions. *Numerische mathematik*, 14(5):403–420, 1970.
- ⁸⁰ Ji Young Hwang. Doppler ultrasonography of the lower extremity arteries: anatomy and scanning guidelines. *Ultrasonography*, 36(2):111, 2017.
- ⁸¹ Verasonics Inc. Verasonics transducer specifications. http://verasonics.com/wp-content/uploads/2015/09/Verasonics-transducer_specifications_sheet_Sept2015.pdf, 2015. Accessed December 10, 2017.
- ⁸² Jacopo Viti, Hendrik J Vos, Nico de Jong, Francesco Guidi, and Piero Tortoli. Detection of contrast agents: Plane wave versus focused transmission. *IEEE transactions on ultrasonics, ferroelectrics, and frequency control*, 63(2):203–211, 2016.
- ⁸³ Bastien Denarie, Thor Andreas Tangen, Ingvild Kinn Ekroll, Natale Rolim, Hans Torp, Tore Bjåstad, and Lasse Lovstakken. Coherent plane wave compounding for very high frame rate ultrasonography of rapidly moving targets. *IEEE transactions on medical imaging*, 32(7):1265–1276, 2013.
- ⁸⁴ Haruhiko Abe, Giuseppe Caracciolo, Arash Kheradvar, Gianni Pedrizzetti, Bijoy K Khandheria, Jagat Narula, and Partho P Sengupta. Contrast echocardiography for assessing left ventricular vortex strength in heart failure: a prospective cohort study. *European Heart Journal—Cardiovascular Imaging*, 14(11):1049–1060, 2013.
- ⁸⁵ Shan Jiang, Sha Liu, and Wenhao Feng. Pva hydrogel properties for biomedical application. *Journal of the mechanical behavior of biomedical materials*, 4(7):1228–1233, 2011.
- ⁸⁶ Christie M Hassan and Nikolaos A Peppas. Structure and applications of poly (vinyl alcohol) hydrogels produced by conventional crosslinking or by freezing/thawing methods. In *Biopolymers—PVA Hydrogels, Anionic Polymerisation Nanocomposites*, pages 37–65. Springer, 2000.
- ⁸⁷ Victor F Humphrey. Nonlinear propagation in ultrasonic fields: measurements, modelling and harmonic imaging. *Ultrasonics*, 38(1-8):267–272, 2000.
- ⁸⁸ International Electrotechnical Commission et al. Iec 62359. *Ultrasonics: Field Characterization Test Methods for the Determination of Thermal and Mechanical Indices Related to Medical Diagnostic Ultrasonic Fields*. 2nd ed. Geneva, Switzerland: International Electrotechnical Commission, 2010.
- ⁸⁹ Paul Morris, Andrew Hurrell, Adam Shaw, Edward Zhang, and Paul Beard. A fabry-pérot fiber-optic ultrasonic hydrophone for the simultaneous measurement of temperature and acoustic pressure. *The Journal of the Acoustical Society of America*, 125(6):3611–3622, 2009.

- ⁹⁰ Food, Drug Administration, et al. Guidance for industry and fda staff information for manufacturers seeking marketing clearance of diagnostic ultrasound systems and transducers. *Silver Spring, MD: Author*, 2008.
- ⁹¹ Prepared by the Safety Group of the British Medical Ultrasound Society. Guidelines for the safe use of diagnostic ultrasound equipment. *Ultrasound*, 18(2):52–59, 2010.
- ⁹² IEC Standard. 60601-2-37. medical electrical equipment-particular requirements for the safety of ultrasonic medical diagnostic and monitoring equipment. *International Electrotechnical Commission, Tech Rep*, 2001.
- ⁹³ FLIR systems Inc. Flir one datasheet. https://www.flirmedia.com/MMC/THG/Brochures/IND_036/IND_036_EN.pdf, July 2015. Accessed April 4th, 2018.
- ⁹⁴ Yann Desailly, Anne-Marie Tissier, Jean-Michel Correas, Frédéric Wintzenrieth, Mickaël Tanter, and Olivier Couture. Contrast enhanced ultrasound by real-time spatiotemporal filtering of ultrafast images. *Physics in Medicine & Biology*, 62(1):31, 2016.
- ⁹⁵ Alfred CH Yu and Lasse Lovstakken. Eigen-based clutter filter design for ultrasound color flow imaging: a review. *IEEE transactions on ultrasonics, ferroelectrics, and frequency control*, 2010.
- ⁹⁶ Ashkan Javadzadegan, Azadeh Lotfi, Anne Simmons, and Tracie Barber. Haemodynamic analysis of femoral artery bifurcation models under different physiological flow waveforms. *Computer methods in biomechanics and biomedical engineering*, 19(11):1143–1153, 2016.
- ⁹⁷ Rolf Holenstein and David N Ku. Reverse flow in the major infrarenal vessels—a capacitive phenomenon. *Biorheology*, 25(6):835–842, 1988.
- ⁹⁸ Charles C Church. Frequency, pulse length, and the mechanical index. *Acoustics Research Letters Online*, 6(3):162–168, 2005.

Appendix A; Study approval letters

Radboud universitair medisch centrum

Concernstaf Kwaliteit en Veiligheid
Commissie Mensgebonden Onderzoek
Regio Arnhem-Nijmegen

628

Mw. M.S. van der Vee
Rijnstate Ziekenhuis afdeling Chirurgie
Wagnerlaan 55
6815 AG ARNHEM

Postbus 9101, 6500 HB Nijmegen
Huispost 628
Geert Groteplein 10
Radboudumc hoofdingang, route 629
T (024) 361 31 54

commissiemensgebondenonderzoek@radboudumc.nl
KvK 41055629/4

Ons Kenmerk
PvW/CMO 288

Datum
12 juni 2018

Titel: Feasibility of ultrasound particle image velocimetry to quantify flow near stented SFA lesions
Dossiernummer: 2018-4355
NL-nummer: NL65760.091.18

Geachte mevrouw van der Vee,

Bijgevoegd treft u aan het positieve oordeel van de CMO Regio Arnhem-Nijmegen over bovengenoemd onderzoek.

Dit betekent dat het onderzoek kan worden uitgevoerd in het centrum dat in het positieve oordeel wordt genoemd nadat de Raad van Bestuur/Directie van het centrum daarvoor toestemming heeft verleend.

Indien het voornemen bestaat het onderzoek ook nog in een ander centrum uit te voeren, dan dient aan de CMO Regio Arnhem – Nijmegen een onderzoeksverklaring (zie website www.ccmo.nl) van het betreffende centrum te worden overlegd. De CMO Regio Arnhem-Nijmegen kan vervolgens het positieve oordeel uitbreiden naar het betreffende centrum.

Bij correspondentie over het onderzoek gelieve titel en dossiernummer te vermelden.

Ik vertrouw erop u met dit schrijven van dienst te zijn en namens de commissie wens ik u succes met de uitvoering van het onderzoek.

Met vriendelijke groet,
Namens de CMO Regio Arnhem-Nijmegen



Drs. R.B. Keus, vicevoorzitter

Betreft Oordeel onderzoeksprotocol
Kenmerk 18.637/(2018-1206-Reijnen)/WvH/nf
Datum 9 juli 2018

De heer M.M.P.J. Reijnen
Postnummer 1190

Raad van Bestuur

Bezoekadres
Wagnerlaan 55 Arnhem

Postadres
Postbus 9555
6800 TA Arnhem

Geachte heer Reijnen,

Hierbij laat ik u weten dat de Raad van Bestuur van Rijnstate kennis heeft genomen van het onderzoeksprotocol, met als titel: "*Feasibility of ultrasound particle image velocimetry to quantify flow near stented SFA lesions*", en van het advies van de Lokale Haalbaarheidscommissie (LHC) over de lokale haalbaarheid van dit onderzoek.

T 088 - 005 7544
F 088 - 005 6900

E-mail
lokalehaalbaarheidscommissie@rijnstate.nl

De Raad van Bestuur oordeelt positief over het onderzoek, na kennis genomen te hebben van de aanmelding in Study Management en de volgende documenten:

www.rijnstate.nl

- Protocol d.d.: 28-05-2018 versie: 2
- Rijnstate patiënteninformatie d.d.: 28-06-2018 versie: 3
- Verzekeringscertificaat
- METC goedkeuring
- Kostenbegroting onderzoek
- CGP certificaat

De Raad van Bestuur stelt als voorwaarde dat bij de uitvoering van bovengenoemd onderzoek de geldende wet- en regelgeving, de WMO, WGBO, de AVG, en de Codes Goed Gedrag en Goed Gebruik (voor zover van toepassing) in acht worden genomen.

De Raad van Bestuur baseert dit oordeel op de volgende overwegingen:

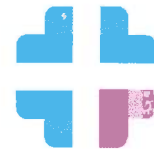
- Het uit te voeren onderzoek is in Rijnstate haalbaar is omdat:
 - de onderzoeker bekwaam is;
 - de personele bezetting op de betrokken afdeling(en) voldoende is voor het uitvoeren van het onderzoek;
 - de geplande inclusie haalbaar lijkt;
 - de kosten voor het onderzoek gedekt zijn.
- Onvoorziene kosten ten behoeve van het onderzoek op de onderzoeker worden verhaald.

De Raad van Bestuur heeft bepaald dat wanneer meerdere centra betrokken worden bij een in Rijnstate geïnitieerd onderzoek, het onderzoek in Rijnstate kan starten nadat het onderzoek van advies is voorzien door de Lokale Haalbaarheidscommissie en akkoord is bevonden door RvB. Vóórdat het onderzoek in de andere centra mag starten, dient ook de contractprocedure te zijn gevolgd en akkoord bevonden.

Verzekeringen

De personen die betrokken zijn bij de uitvoering van voornoemd onderzoek in Rijnstate vallen onder de aansprakelijkheidsverzekering van uitvoerders van Rijnstate.

Betreft Oordeel onderzoeksprotocol
Blad 2/2



Rijnstate

De proefpersonen in Rijnstate vallen onder de WMO-proefpersonenverzekering van Rijnstate bij MediRisk.

Dit positieve oordeel verliest geldigheid indien met het uitvoeren van het wetenschappelijk onderzoeksvoorstel waarop het betrekking heeft, niet is begonnen binnen één jaar nadat dit besluit is genomen (Reglement LHC 11.2).

De onderzoeker dient de Raad van Bestuur via melding aan LHC op de hoogte te stellen van het einde van het onderzoek (einde gegevensverzameling) en van enig amendement op dit onderzoek.

Het studienummer van deze studie is 2018-1206, gelieve dit nummer in de correspondentie te vermelden. Ook is dit nummer toegevoegd aan het EPD zodat patiënten die geïncludeerd worden in deze studie hieraan gekoppeld kunnen worden.

In het vertrouwen u namens de Raad van Bestuur voldoende te hebben geïnformeerd, tekent,

Met vriendelijke groet,



Prof. Dr. W.H. van Harten
Voorzitter Raad van Bestuur

Bijlage: Samenstelling Lokale Haalbaarheidscommissie

Lokale Haalbaarheidscommissie

Telefoon 088-005 7870
Fax 088-005 8820
E-mail lokalehaalbaarheidscommissie@rijnstate.nl

Samenstelling Lokale Haalbaarheidscommissie

Mw. dr. C. Meeuwis, radioloog	voorzitter
Mw. drs. E.G.M. Pallast	secretaris
Mw. N.B. van Dijk, spoedeisende hulparts	lid
Dhr. Dr. R.R.J.P. van Eekeren, chirurg	lid
Mw. dr. P.M.G. Filius, ziekenhuisapotheker	lid
Dhr. drs. J. Holkenborg, spoedeisende hulparts	lid
Dhr. dr. H. de Waard, klinisch chemicus	lid